AD-A169 119 SEMICONDUCTOR/INSULATOR FILMS FOR CORROSION PROTECTION 1/1
(U) CONNECTICUT UNIV STORRS DEPT OF ELECTRICAL
ENGINEERING AND COMPUTER SCIENCE F C JAIN OCT 85
UNCLASSIFIED NADC-86020-60 N62269-83-M-3295 F/G 20/12 NL

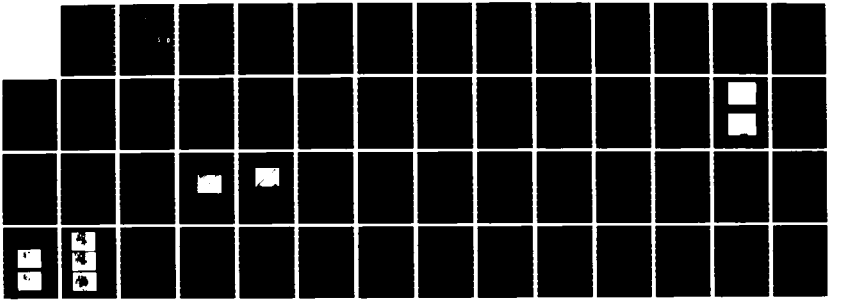

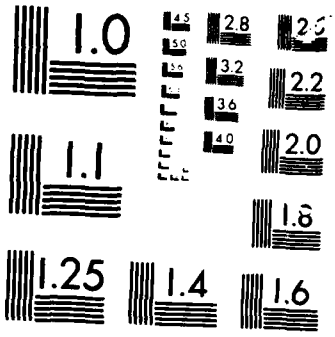

(12)

REPORT NO. NADC-86028-60

AD-A169 119

SEMICONDUCTOR/INSULATOR FILMS FOR CORROSION PROTECTION

F. C. Jain
The University of Connecticut
Electrical Engrg. & Computer Science, U-157
Storrs, Connecticut 06268

OCTOBER 1985

FINAL REPORT
NADC Contract N62269-83-M-3295

Approved for Public Release; Distribution Unlimited

Prepared for
NAVAL AIR DEVELOPMENT CENTER
Warminster, PA 18974-5000

NOTICES

REPORT NUMBERING SYSTEM - The numbering of technical project reports issued by the Naval Air Development Center is arranged for specific identification purposes. Each number consists of the Center acronym, the calendar year in which the number was assigned, the sequence number of the report within the specific calendar year, and the official 2-digit correspondence code of the Command Office or the Functional Directorate responsible for the report. For example, Report No. NADC-86015-20 indicates the fifteenth Center report for the year 1986, and prepared by the Systems Directorate. The numerical codes are as follows:

CODE	OFFICE OR DIRECTORATE
00	Commander, Naval Air Development Center
01	Technical Director, Naval Air Development Center
02	Comptroller
10	Directorate Command Projects
20	Systems Directorate
30	Sensors & Avionics Technology Directorate
40	Communications and Navigation Technology Directorate
50	Software Computer Directorate
60	Aircraft & Crew Systems Technology Directorate
70	Planning Assessment Resources
80	Engineering Support Group

PRODUCT ENDORSEMENT - The discussion or instructions concerning commercial products herein do not constitute an endorsement by the Government nor do they convey or imply the license or right to use such products.

UNCLASSIFIED

SECURITY CLASSIFICATION OF THIS PAGE

REPORT DOCUMENTATION PAGE

1a REPORT SECURITY CLASSIFICATION: Unclassified	1b RESTRICTIVE MARKINGS
2a SECURITY CLASSIFICATION AUTHORITY	3 DISTRIBUTION AVAILABILITY OF REPORT: Approved for Public Release; Distribution is Unlimited
2b DECLASSIFICATION/DOWNGRADING SCHEDULE	
4 PERFORMING ORGANIZATION REPORT NUMBER(S): NADC-86028-60	5 MONITORING ORGANIZATION REPORT NUMBER(S): N/A
6a NAME OF PERFORMING ORGANIZATION: Naval Air Development Center; 6b OFFICE SYMBOL (If applicable)	7a NAME OF MONITORING ORGANIZATION: N/A
6c ADDRESS (City, State, and ZIP Code): Warminster, PA 18974	7b ADDRESS (City, State, and ZIP Code): N/A
8a NAME OF FUNDING/SPONSORING ORGANIZATION: Naval Air Systems Command; 8b OFFICE SYMBOL (If applicable)	9 PROCUREMENT INSTRUMENT IDENTIFICATION NUMBER: Contract No. N62269-83-M-3295
8c ADDRESS (City, State, and ZIP Code): Washington, D.C. 20361	10 SOURCE OF FUNDING NUMBERS: PROGRAM ELEMENT NO; PROJECT NO; TASK NO; WORK UNIT ACCESSION NO

11 TITLE (Include Security Classification)

Semiconductor/Insulator Films for Corrosion Protection

12 PERSONAL AUTHOR(S): F.C. Jain

13a TYPE OF REPORT	13b TIME COVERED	14 DATE OF REPORT (Year, Month, Day)	15 PAGE COUNT
Final	FROM ____ TO ____	1985 October	

16 SUPPLEMENTARY NOTATION

17 COSATI CODES			18 SUBJECT TERMS (Continue on reverse if necessary and identify by block number)
FIELD	GROUP	SUB-GROUP	

19 ABSTRACT (Continue on reverse if necessary and identify by block number)

Aluminum surfaces exhibit significantly improved corrosion protection when they are coated with suitable semiconductor/insulator thin films. These coatings, generally realized in Metal-Semiconductor (MS) or Metal-Insulator-Semiconductor (MIS) structural configurations, given rise to an interfacial electric field which acts as an effective built-in electronic barrier. This active barrier significantly impedes the transfer of electrons from the aluminum surface to foreign species which cause oxidation by accepting the electrons. Anodic polarization data on numerous samples fabricated in both MS [e.g. Al-Indium Tin Oxide (ITO)] and MIS [e.g. Al-SiO_2-ITO] configurations have demonstrated the protective nature of the built-in active electronic barrier. In particular, we have observed a rest potential of -1.126 volts (1% NaCl, 2pH solution) for Al-SiO_2-pITO samples in polarization tests. The electronic barrier heights have been shown to increase with: (1) the presence of a thin (20-100 Å) SiO_2 layer at the metal-semiconductor interface; and (2) the energy gap of ITO which depends upon the indium content. A comparison of these results with data obtained on plasma-deposited Al-Si_3N_4 samples is also presented.

20 DISTRIBUTION AVAILABILITY OF ABSTRACT	21 ABSTRACT SECURITY CLASSIFICATION
☐ UNCLASSIFIED/UNLIMITED ☒ SAME AS RPT ☐ DTIC USERS	Unclassified
22a NAME OF RESPONSIBLE INDIVIDUAL: V.S. Agarwala	22b TELEPHONE (Include Area Code) / 22c OFFICE SYMBOL

DD FORM 1473, 84 MAR — 83 APR edition may be used until exhausted. All other editions are obsolete.

SECURITY CLASSIFICATION OF THIS PAGE

TABLE OF CONTENTS

		Page
	LIST OF TABLES	ii
	LIST OF FIGURES	ii
I.	INTRODUCTION	1
II.	THEORY OF ACTIVE ELECTRONIC BARRIER FORMATION AT METAL-SEMICONDUTOR/INSULATOR INTERFACES	2
	II.1 Metal-Semiconductor Interfaces	4
	II.2 Metal-Oxide (Insulator)-Semiconductor Interfaces	4
III.	ACTIVE ELECTRONIC BARRIER SYSTEMS FABRICATED: EXPERIMENTAL	6
	III.1 Selection of Semiconductor/Insulator Coating Systems	6
	III.2 Structures Fabricated	7
	III.3 Fabrication Techniques	7
	III. 3.A Substrate Preparation	7
	III. 3.B Semiconductor Coatings: Deposition of SnO_2 and ITO Films	9
	III. 3.C Insulator Films	15
IV.	RESULTS	15
	IV.1 Characterization of ITO, SnO_2, and Si_3N_4 Coatings	15
	IV. 1.A Physical Characterization	15
	IV. 1.B Optical Characterization of SnO_2 and ITO Coatings	17
	IV. 1.C Electronic Measurements	21
	IV.2 Corrosion Testing	26
V.	DISCUSSION	32
VI.	CONCLUSIONS	36
VII.	FUTURE WORK	37
	ACKNOWLEDGEMENTS	39
	REFERENCES	40

LIST OF TABLES

Table	Title	Page
1	Chemical Reactions	14
2	Chemical Composition of ITO Films	17
3	Four Point Probe Resistivity Measurements	22
4	Anodic Polarization Results	26
5	Weight Loss Measuremnts on CVD Deposited Samples	32
6	Effect of Increased Indium Content in ITO	36

LIST OF FIGURES

Figure	Title	
1	Electron Transfer During Oxidation	1
2	Electronic Energy Band Diagram of a Metal-Oxide System (Passive Electronic Barrier)	3
3	Electronic Barrier Due to a Built-In Electric Field	4
4	Electronic Barrier Formation at a Metal-pSemiconductor Interface	5
5	Structures Fabricated to Test Corrosion Prevention	8
6(a)	Schematic of a Indium-Tin-Oxide(ITO) Chemical Vapor Deposition Reactor	10
6(b)	Controlled Ambient spray injection CVD ITO reactor	11
7	Spray Pyrolysis Apparatus	13
8	Schematic of a SiO_2 Deposition Reactor	16
9(a)	SEM Micrograph of CVD Deposited ITO Film	18
9(b)	SEM Micrograph of a Spray CVD Deposited ITO Film	18
10	The Absorption Edge of Indium Tin Oxide	19
11	The Absorption Edge of Tin Oxide	20
12	V-I Characteristics Test Setup	21
13	Current-Voltage Characteristic of an Al-ITO/Quartz Sample	23
14	Current-Voltage Characteristic of an Al-ITO/Quartz Sample	24
15(a)	Current Volatge Characteristic of CVD Al-ITO Sample (Dark Condition)	25

Figure	Title	Page
15(b)	Current-Voltage Characteristic of CVD Al-ITO Sample (Under Illumination)	25
16	Polarization Characteristics of Commercial Purity Aluminum Substrates	27
17	Polarization Characteristics of High Purity Aluminum Substrates	28
18	Polarization Characteristics of Aluminum Alloy (#7075-T6) Substrates	28
19	Polarization Characteristic of a Commercial Purity Aluminum Substrate(with Composite ITO/TO Film)	29
20	Polarization Characteristic of a Scratched Aluminum Substrate(Commercial Purity)	30
21	Polarization Characteristics of CVD Deposited Low Indium Content ITO Samples	31
22	Undercutting of ITO Films at Large Pinhole Sites (Pictures Taken After Exposure to 1% NaCl, 2pH Solution for Following Durations: (a) 15 Minutes; (b) 45 Minutes; (c) 75 Minutes; (d) 105 Minutes; and (e) 135 Minutes.)	34

I. INTRODUCTION

The oxidation of a metallic surface involves a net transfer of electrons from the metal to a foreign species such as oxygen, sulphur etc. Oxidation is favored energetically as it results in a decrease in the free energy of the system. The reaction is commonly expressed[1] as:

Oxidation:

$$Me \rightarrow Me^{z+} + z \text{ electrons}$$

Reduction:

$$O_2 + z \text{ electrons} \rightarrow \frac{z}{2} O^{2-}$$

Net:

$$Me + O_2 \rightarrow MeO_{z/2}$$

A schematic illustration of the oxidation process is shown in Fig. 1. Reactions involving chloride, nitride, and sulphide formations, which generally occur in the environment, can be expressed similarly. Theoretically, the interactions at a solid surface with the species available in a given ambient are determined by its chemical and electronic properties.

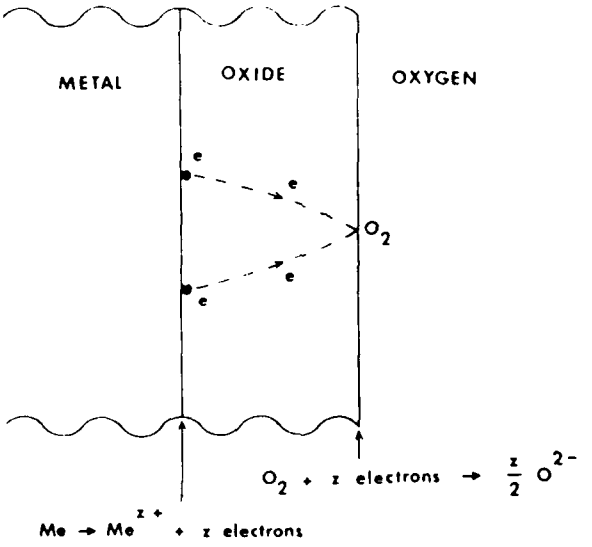

Fig. 1. Electron Transfer During Oxidation
(only the electron transfer is specifically shown).

Foreign species may interact and subsequently be adsorbed at the surface of a solid in a variety of ways. For instance, a species may be physiosorbed, chemisorbed (via ionosorption or local chemical bonding), or form a new phase (e.g. oxidation on a metallic surface). Adsorption of oxygen on clean semicon ductor and metallic surfaces has been a topic of intense experimental (surface sepctroscopies) and theoretical (local density of states LDOS calculations) investigations.[2-6] The chemical and electronic properties of absorption on clean surfaces are described by atomistic (surface site or surface molecule), and band (surface state or rigid band) models. Morrison[7] and Schreiffer and Soven[8] have combined the two approaches by considering the chemical bonding and the energy band interaction. The nature of the chemical bonding of a foreign species to the solid surface determines whether the surface corrodes, acts as a catalyst in a chemical reaction, or remains relatively inert (passivated) in an ambient.

Metallic oxides are generally used as protective coatings to inhibit corrosion. In some cases (e.g. Ni/NiO, Cr/Cr_2O_3) the native oxide does not grow above a thickness value of 10-15 Å at room temperature, regardless of exposure time to the atmospheric conditions. In other cases, the oxidation takes place continually. The corrosion resistance of oxide coatings, grown naturally or intentionally (using one of several methods available), depends on the chemical and electronic structure, the thickness, and the porosity of the oxide layer. SiO_2, NiO, Cr_2O_3 are well known examples of naturally occurring protective thin oxides on Si, Ni, and Cr surfaces, respectively. In addition, growing oxide on Al, Ti, and Ta surfaces using anodic oxidation is a common practice to protect these metals against corrosion.[1,9-11] The theory of anodic oxidation of metals has been reviewed by Wagner.[12] Coatings of silicides, aluminides, and nitrides have also been used as protective layers.[1] Schneider, Bauer, and Grunling[13] have studied the failure mechanisms of Si, Cr, and Ni-Cr-Si coatings for turbine applications. Among these, silicon coatings with native SiO_2 layers have been found to be the most protective against high temperature corrosion and oxidation. However, the Ni-Cr-Si coatings were found to be more desirable due to their ductility, toughness, and reasonable corrosion resistance. The theory of metal oxidation has recently been reviewed by Fromhold.[14,15]

II. THEORY OF ACTIVE ELECTRONIC BARRIER FORMATION AT METALLIC SURFACES

The ability of an oxide or nitride layer to prevent corrosion is dependent upon its electrical resistivity. The higher the electrical resistance of the oxide layer the more effective it will be in preventing electron transfer. In general, the current flow due to the oxidation of a metal surface will depend on the resistance/impedance of the oxide layer. The higher the resistance, the better will be the protection. The electrical resistance of an oxide layer depends upon many factors including the oxide thickness, as well as the electronic (defects states in the energy gap etc.) and physical (pin holes etc.) qualities of the oxide. Fig. 2 shows the energy band diagram of an oxide with defect states in the energy gap. Fromhold[14,15] has summarized the mechanisms responsible for electronic and ionic current flow during oxidation in oxides ranging in thickness from 10 Å to 100 microns. This type of protection can be viewed as a passive electronic barrier at the metal surface.

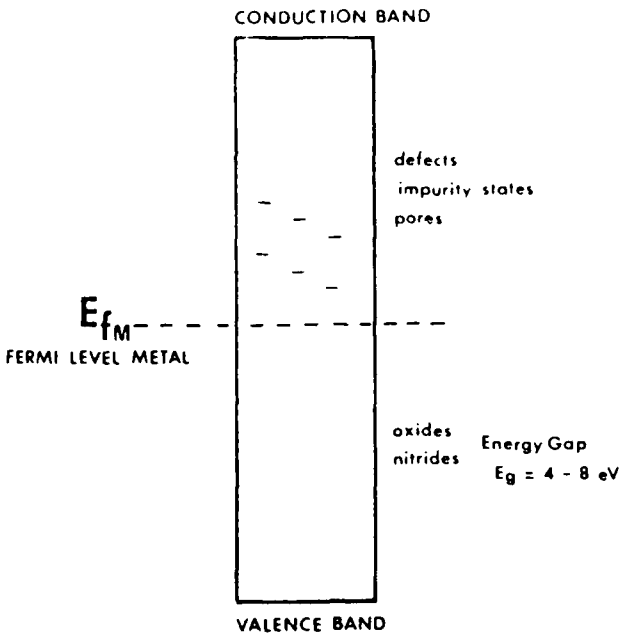

Fig. 2 Electronic Energy Band Diagram of a Metal - Oxide System (passive electronic barrier)

This paper presents a new approach to corrosion prevention. Rather than utilizing a simple passive barrier, we may create conditions at the metal surface such that it hosts a built-in electric field. The presence of such an electric field E, as shown in Fig. 3, will impede the transfer of electrons from the metal surface. Electrons now see a retarding force which prevents their transfer to the oxidizing species. This force can be expressed as $F = - e E$, where e is the magnitude of the electron charge. It should be noted that the interfacial electric field is not due to any externally applied voltage, rather it is built-in at the metal-semiconductor. Metallic surfaces host positive dipole layers when they are interfaced with appropriately doped semiconductors to form metal and metal-semiconductor and metal-oxide (insulator)-semiconductor structures.[16] These interfacial space charge layers result in a built-in electric field and cause bending of the electronic energy bands. The net band bending is defined as the active electronic barrier. This novel approach to corrosion prevention was first proposed by Jain.[17] It may be added that by properly selecting the semiconductor coating material for a metal surface one can realize both the traditional passive as well as the novel active barriers. The formation of an active electronic barrier is described next.

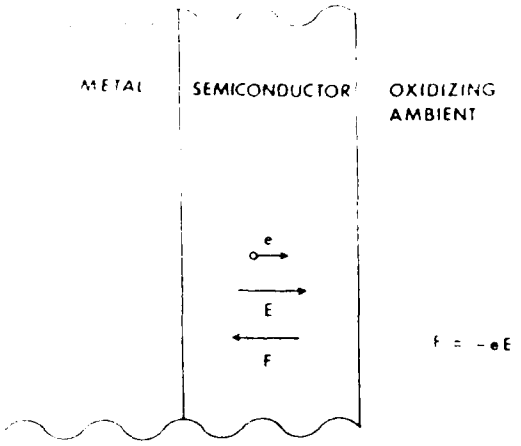

Fig. 3 Electronic Barrier Due to a Built-In Electric Field

II.1 Metal-Semiconductor Interfaces

The behavior of a metal-semiconductor interface, commonly called a Schottky barrier, is known to depend on the work function of the metal, the conductivity type, the carrier concentration, and the energy gap of the semiconductor.[16,18-20] Fig. 4 shows the energy band diagram, charge distribution, and electric field profile in a metal-p type semiconductor interface. It may be added that n-type semiconductors will also form barriers with metals.

The magnitude of the electronic barrier is dependent upon the choice of metal (i.e. its work function) and the properties of the semicondutor. The presence of impurities, which can act as traps for electrons and holes in a p-type semiconductor layer, are also known to affect the barrier height. For a given metal, the barrier height of a metal-semiconductor interface is dependent upon the doping levels and the energy gap of the semiconductor. In general, wider energy gap semiconductors yield higher barrier. Recently, Brillson[21] and others have investigated the barrier formation in its initial phases using electron loss and other spectroscopic techniques.

II.2. Metal-Oxide (Insulator)-Semiconductor Interfaces

A metallic surface can also develop a positively charged dipole layer and the associated active electronic barrier in a metal-oxide(insulator)-p semiconductor (MOS) configuration. The physics of the barrier formation depends upon the thickness of the oxide. The manifestation of the electronic barrier in thick oxide (> 150 Å) systems is similar to those of conventional MOS

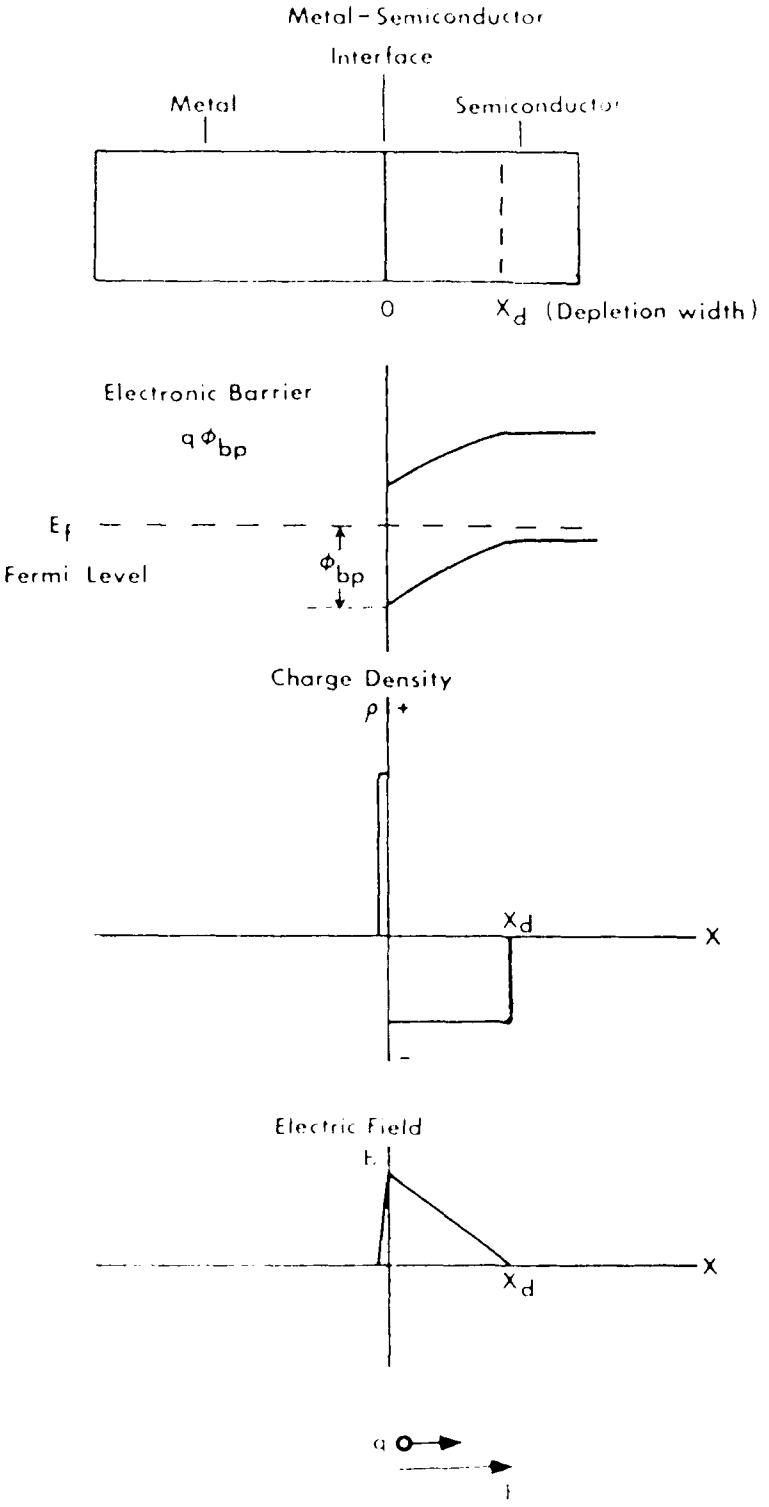

Electric field impeding the transfer of electrons

Figure 4. Energy band diagram of a metal-p semiconductor interface

devices used in Si integrated circuit technology.[16,19] Thick oxide MOS structures are not treated in this paper. Structures utilizing oxide(insulator) thickness in the range of (20-100 Å) are generally known as MIS structures. These systems behave similarly to the metal-semiconductor systems described above. However, the barrier has been found to be larger in MIS than in MS configurations.[24-26] For instance, we have found that the barrier height is increased in Al-nSi and Au-nGaAsP interfaces with the introduction of a thin 20-30 Å SiO_2 layer. Reference is made to Jain and Marciniec,[25] and Jain and Nichols[26] for detailed conditions of barrier enhancement in Schottky type MOS structures.

The active electronic barrier inhibits the net transfer of electrons from the metal surface to the oxidizing species, resulting in a lower probability of oxidation/corrosion. Additionally, the electronic barrier may help in regions having micropores and pinholes in the semiconductor layer. In these regions we expect a finite electric field (due to field fringing effects) to retard the transfer of electrons.

III. ACTIVE ELECTRONIC SYSTEMS FABRICATED - EXPERIMENTAL

III.1. Selection of Semiconductor/Insulator Coating Systems

The electronic barrier at the aluminum surface is realized by depositing a thin coating of n or p-type inidum tin oxide (ITO). ITO films can be grown in n-doped or p-doped form depending on the reactor growth conditions. The indium tin oxide was selected for several reasons including:

a. adjustable large energy gap (3.5 to 4.0eV for films having higher In/Sn ratio),

b. potentially controllable n- and p-type doping (in contrast to doped polyacetylene, phthalocynine etc.),

c. stable and durable film coatings (it has been recently reported that phthalocyanine[27] and doped polyacetylene[28] are not stable under illuminated and oxidizing environments, respectively),

d. adaptability to chemical vapor deposition (CVD) and spray deposition techniques.

In addition to the active electronic barrier at the metal interface, the ITO film also acts as a passive barrier due to its high resistivity. The resistivity/passivity of metals and semiconductor has been the topic of a recent conference in France.[29]

The use of a thin (300-100 Å) SiO_2 insulator layer in a MIS configuration is chosen for two reasons: (1) to enhance the electronic barrier at Al-ITO interfaces; and (2) to protect Al alloys (e.g. 7075-T6) from being attacked by reaction products in the ITO CVD reactor. A final Si_3N_4 coating was used to physically protect the ITO surface against wear and abrasion. It will be shown in the next section that the active electronic barrier is the primary mechanism preventing the corrosion of Al substrates, and that the Si_3N_4 coatings without the ITO film is a poor corrosion inhibitor. The sole purpose of the nitride coating is to protect the surface against wear.

III.2 Structures Fabricated

The semiconductor (ITO) and insulator (SiO_2, Si_3N_4) films were deposited in a variety of configurations. Fig. 5 shows the metal-semiconductor and metal-thin insulator-semiconductor structures fabricated using the ITO, SiO_2 and Si_3N_4 films. It should be noted that a thin layer of aluminum oxide was grown on all the Al substrates prior to the deposition of other coatings.

The aluminum substrates were prepared from several different grades of aluminum and aluminum alloys. For example, commercial purity as well as high purity aluminum were used for polycrystalline substrates. High pruity, single crystal aluminum substrates were also used. In the case of aluminum alloy, the 7075-T6 alloy was used. The ITO semiconductor coatings were deposited in the thickness range of 0.1-0.3μm. The SiO_2 coating thickness varied between 20-100 Å. The outermost Si_3N_4 coatings were approximately 0.75μm thick.

III.3. Fabrication Techniques

Aluminum and aluminum alloy sample surfaces were prepared using mechanical, chemimechanical, and chemical polishing techniques. A thin layer of native aluminum oxide was grown in a dry oxygen ambient at the relatively low temperature range of 300-375°C,. Aluminum substrates with a thin native oxide were then deposited with either thin SiO_2 or ITO films depending on the structural configurations desired.

III.3.A. Substrate Preparation

All aluminum substrates (including Al alloy) were mechanically and chemically polished to a mirror-like finish prior to film deposition. The following procedure was used:

1) Boil in Trichloroethylene
2) Acid etch in 10% Hydrofluoric acid (5 seconds)
3) Mechanical lapping
4) Boil in Trichloroethylene
5) Mechanical polish with 5 micron alumina polish
6) Mechanical polish with 0.3 micron alumina polish
7) Mechanical polish with 0.05 micron alumina polish
8) Mechanical polish in ethylene glycol
9) Wash in distilled water
10) Boil in Trichloroethylene
11) Chemical microetch in 10% phosphoric acid
12) Rinse in distilled water

After polishing, the substrates were placed in an oxide furnace for aluminum oxide growth. The temperature was mainted at 300-375°C in a pure oxygen environment. After 15-20 min., the substrates were removed. At this point, a thin layer of approximately 20 Å of Al_2O_3 covered the aluminum surface.

Aluminum substrates with a thin native oxide were then processed for SiO_2, ITO, and silicon nitride depositions. These growths are described in the next two sections.

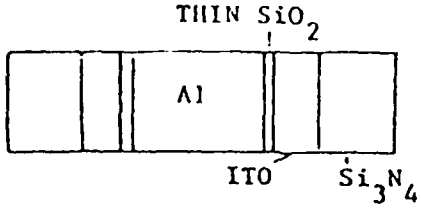

1. Al-Thin SiO_2-ITO-Nitride

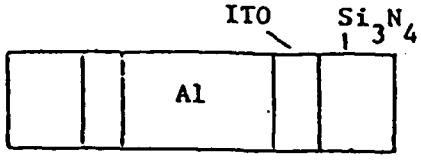

2. Al-ITO-Si_3N_4

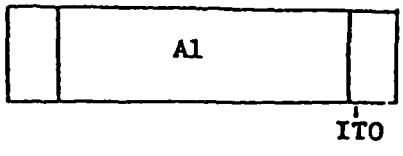

3. Al-ITO

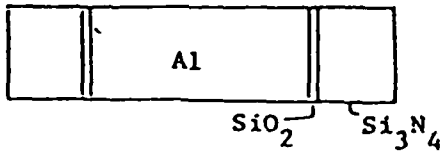

4. Al-Thin SiO_2-Si_3N_4

FIGURE 5 - Structures fabricated to test corrosion prevention

III.3.B Semiconductor Coatings: Deposition of SnO_2 and ITO Films

The semiconductor films of Indium Tin Oxide (ITO) and Tin Oxide (SnO_2) were deposited by three techniques: 1) chemical vapor deposition (CVD), 2) spray injection chemical vapor deposition, and 3) air spray pyrolysis.

Chemical Vapor Deposotion Reactor

Fig. 6a shows the CVD reactor which was utilized in the early phases of the project work. The system features separate feed lines for the reactant chemicals to allow for precise control of the film deposition. Indium chloride, water, and ethanol were mixed to form one reactant solution, while anhydrous tin chloride was used for the second solution. By controlling the flow rates of the two reactant solutions, either SnO_2 or ITO films could be fabricated. It should be noted that the anhydrous $SnCl_4$ was contained in a methylene chloride base, which initiated a competing reaction in the CVD reactor.

Spray Deposition Reactors

Two types of reactor systems were developed to spray deposit the semiconductor films. The first system utilized a controlled ambient environment for a chemical vapor deposition. Films grown in this reactor were of very high quality and were used for laboratory characterization. The second reactor system was developed to simulate a commercial application process. This system utilized an open air environment with a high pressure spray gun. The films grown in this system were very thick, although of somewhat lower quality.

The spray deposition technique was developed to increase the film uniformity and thickness. In addition, the composition and quality of the deposited films could be easily controlled by changing the makeup of the spray solution. The spray solution contained varying amounts of $InCl_3$, $SnCl_4 \cdot 5H_2O$, CH_3CH_2OH, and H_2O. The amount of indium in the deposited ITO films could be increased or decreased by altering the concentration of $InCl_3$ in the starting solution. This allowed for an effective means of tailoring the bandgap of the semiconductor film. The films deposited by this method were found to be uniform and semiconducting. The two systems are described in detail below.

Spray Injection Chemical Vapor Deposition Reactor

Figure 6b shows a schematic diagram of this system. This system utilizes a controlled ambient environment in which the temperature is precisely controlled. The starting solution is aspirated through the injector nozzle using a high pressure nitrogen gas stream. The resultant mist is sprayed into the reactor where it is preheated at the nozzle tip and then vaporized in zone I. The aluminum substrate is placed in a quartz holder which is located at the zone I/zone II boundry. The temperature of zone I is typically maintained at 575°C while zone II is at 500°C. This difference creates a temperature gradient which enhances the chemical vapor deposition on the aluminum substrate. The actual substrate temperature is typically 390-430°C. The composition of the ITO films is varied by changing the spray solution makeup and by varying the zone temperature. The

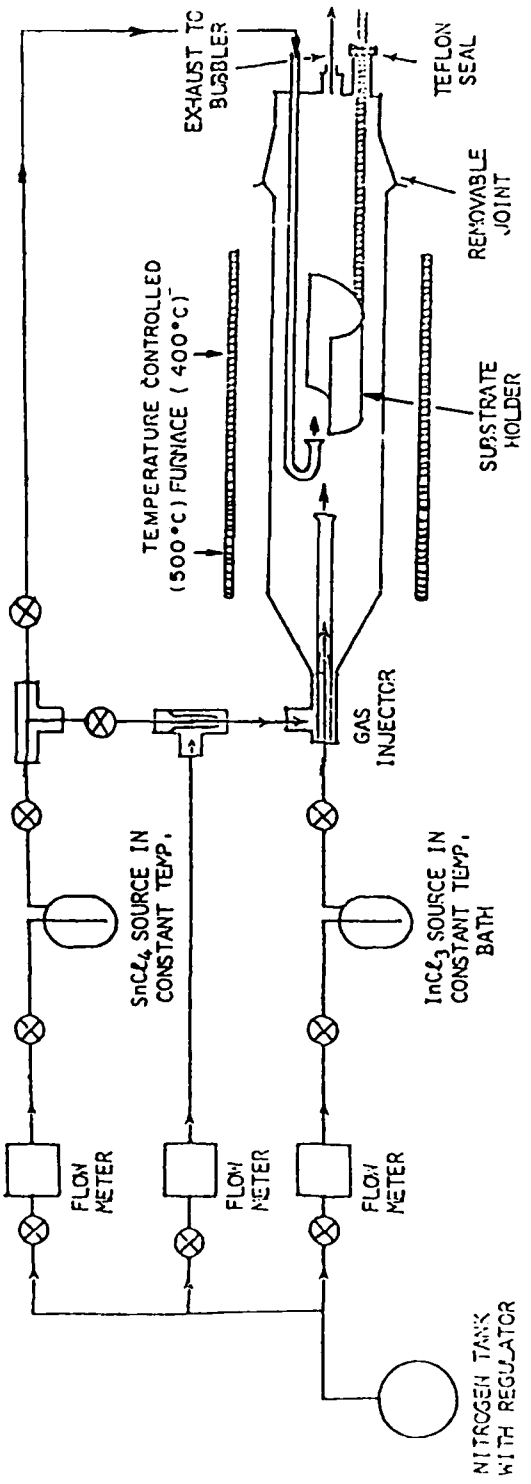

FIGURE 6a - Schematic of Indium-Tin-Oxide (ITO)

Chemical Vapor Deposition reactor

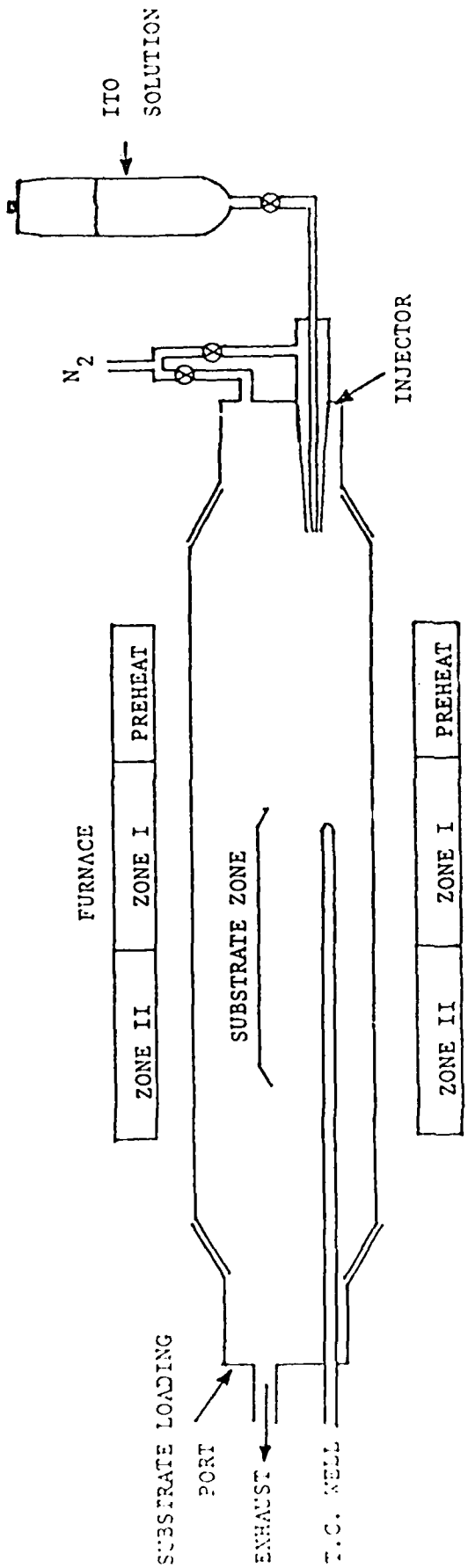

FIGURE 6b - Controlled ambient spray injection CVD ITO reactor

thickness of the film is determined by the quantity of solution injected and the precise location of the substrate.

The films deposited in this reactor were of very high quality. Due to the controlled ambient environment, the number of defects and impurity states in the semiconductor films could be minimized. These films were used for analysis and characterization (i.e.: Auger, SEM analysis, spectrophotometric analysis, and electronic characterization).

Air Spray Reactor System

A second spay deposition system was developed with the goal of simulating a commercial type application of the semiconducting films. This system is shown schematically in figure 7. In this reactor, the spray deposition takes place in an open air environment. The air if filtered through a submicron filter, but is held at room temperature. In order to achieve the high substrate temperature required for the reaction, the substrate is placed on a hot plate at approximately 390-430^{o}C. The starting solution is aspirated with nitrogen and sprayed directly on the aluminum substrate. The height and angle of the spray nozzle is fully adjustable to optimize film thickness and quality.

The films deposited in this "open-air" system were typically very thick and uniform. However, due to the influence of impurities in the ambient, the films did not form an electronic barrier as large as those deposited in the CVD reactor.

ITO and SnO_2 Deposition Reactions

ITO Chemical Reaction

The chemical reaction which occurs in the ITO CVD and ITO spray deposition processes is an oxidation-reduction reaction. Table 1 gives the reaction in detail. The reactants used in the spray deposition solution were 3.9M $InCl_3$, $SnCl_4 .5\ H_2O$ (hydrated crystals), CH_3CH_2OH (ethanol), and water. A typical mixture used to yield an indium-rich film of ITO consists of:

0.5 cc 3.9M $InCl_3$

1.25 g $SnCl_4 .5\ H_2O$

7 cc CH_3CH_2OH

3 cc H_2O

The resultant solution is then sprayed through the injection nozzle.

Tin-Oxide Chemical Reaction

In forming tin-oxide, the $InCl_3$ is deleted from the list of reactants above. A typical solution mix is:

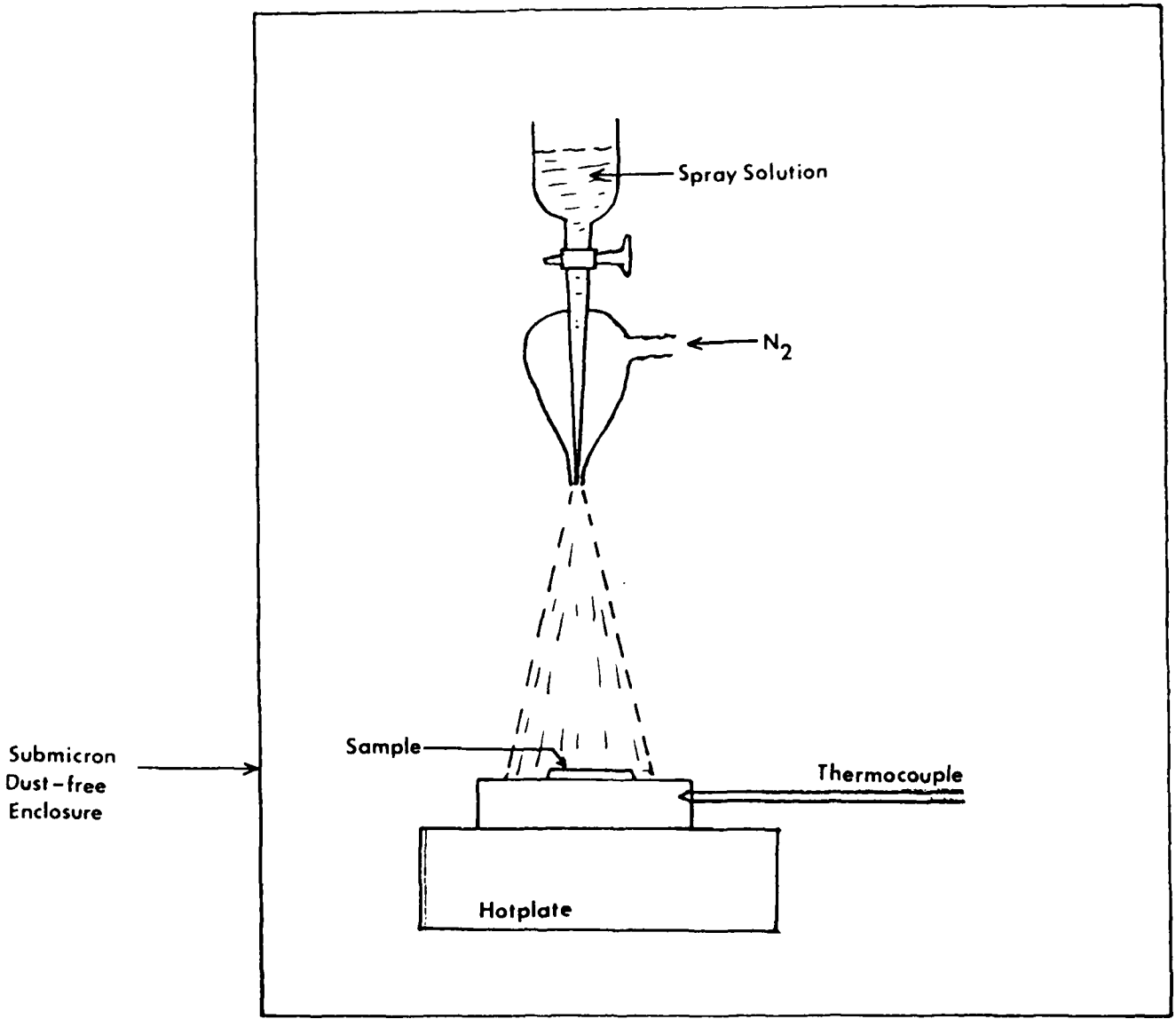

FIGURE 7 - SPRAY PYROLYSIS APPARATUS

TABLE 1 - Chemical reactions

ITO Spray Deposition Reaction

Oxidation

$$CH_3CH_2\text{-}\ddot{O}H \longrightarrow CH_3\,\underset{\underset{:O:}{\|}}{C}\,-\,H + 2H^+ + 2e^-$$

Reduction

$$Sn^{+4} + 2e^- \longrightarrow Sn^{+2} \qquad [E^O = {}^+0.15V \text{ at } 25°c \text{ for } Sn^{+4}]$$

Total Reaction (Aldehyde)

$$2In^{+3}Cl_3 + Sn^{+4}Cl_4 \cdot 5H_2O + CH_3CH_2\text{-}\ddot{O}H \xrightarrow{400°C,N_2} 2In^{+3} + Sn^{+4} + 10Cl^- + 10H^+ + 2H^+ + 2e^- + 5O^-$$

$$+CH_2\,\underset{\underset{:O:}{\|}}{C}\,-\,H$$

$$\longrightarrow In_2^{+3}\,Sn^{+2}\,O_4^{-2} + CH_3\underset{\underset{O}{\|}}{C}H + 10\,HCl + H_2O$$

SnO_2 Formation in absence of significant $InCl_3$

$$SnCl_4 + 2H_2O \longrightarrow SnO_2 + 4HCl$$

Methylene Chloride competing reaction (Ethanol production)

$$2CH_2Cl_2 + H_2O \longrightarrow CH_2CH_3OH + 2Cl_2 + \text{heat}$$

and $$2Cl_2 + 2H_2O \longrightarrow 4HCl + O_2$$

1.25 g $SnCl_4.5\ H_2O$

3.0 cc H_2O

7.0 cc CH_3CH_2OH

Tin-oxide films can be formed at a lower temperature than ITO films. The minimum reaction temperature is approximately 350°C. However, the SnO_2 films have a lower energy bandgap than ITO and do not form as large an electronic barrier. The reaction which occurs in SnO_2 deposition is also shown in Table 1. Also given at the bottom of Table 1 is the competing reaction involving methylene chloride which occurred in the CVD reactor (with separate feed solutions of $InCl_3$ and anhydrous $SnCl_4$).

C. Insulator Films

Silicon Dioxide Growth

Fig.8 gives a schematic representation of the SiO_2 reactor. The deposition of SiO_2 involves the pyrolytic decomposition of tetraethylorthosilicate (TEOS) at above 700°C. However, the samples are kept in a lower temperature zone ranging betweens 450-500°C. The reaction resulting in SiO_2 deposition is as follows.

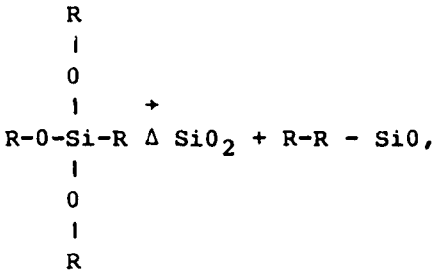

Where R is the hydrocarbon radical.

IV. RESULTS

IV.1 Characterizatio of ITO, SnO_2, SiO_2, and Si_3N_4 Coatings

IV.1.A. Physical Characterization

Important parameters in the physical characterization are:

a. chemical composition

b. grain size

c. film thickness

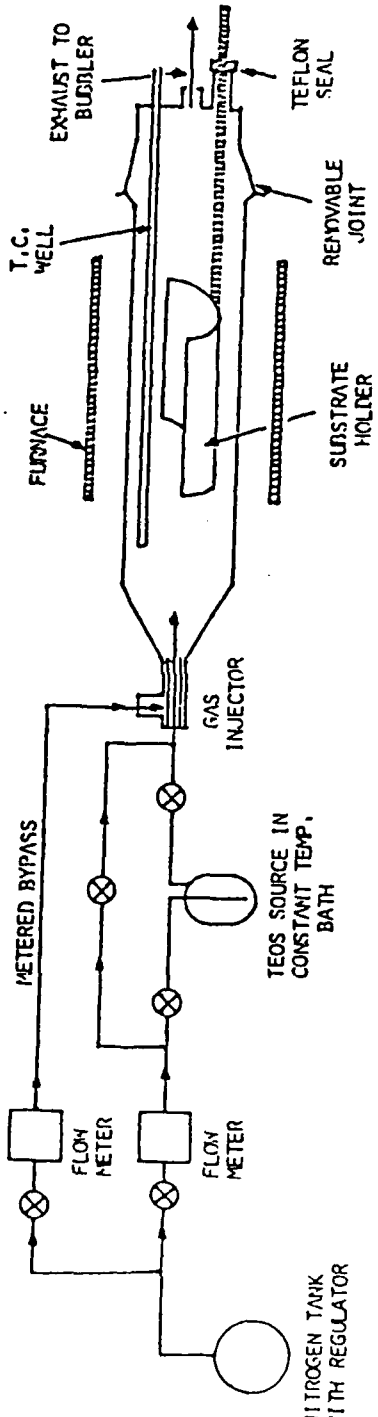

FIGURE 8 - SCHEMATIC OF SiO_2 DEPOSITION REACTOR

The chemical composition is determined using energy and wavelength dispersive techniques such as EDAX and WDAX. These analytical techniques are available as an attachment to a scanning electron microscope. In addition, an Auger depth profiling setup (at the United Technologies Research Center) is used for additional information on the deposited films. The scanning electron and optical microscopes were used to determined the grain size of ITO films.

The WDAX data is shown in Table 2.

Table 2. - Chemical Composition of ITO Films

Sample	Film Structure	Composition	Molar In/Sn ratio	Growth Method
#1	ITO/Si	$In_{.26}Sn_{.42}O_{.75}$	0.62	Injection CVD
#2	ITO/SiO_2/Al	$In_{.003}Sn_{.14}O_{.67}$	0.002	CVD
#3	ITO/SiO_2/Al	$In_{.28}Sn_{.46}O_{.74}$	0.61	Injection CVD
#4	ITO/SiO_2/Al	$In_{.34}Sn_{.44}O_{.47}$	0.78	Injection CVD

The SEM micrographs of ITO films on Si and Al substrates are shown in Figs. 9(a) and 9(b), respectively. Fig. 9(a) shows an ITO film deposited by the CVD technique. The film surface appears extremely fine grained with little evidence of pinholes. Fig. 9(b) shows a spray injection deposited ITO film. The film structure is coarser and shows some pinholes.

IV. 1.B Optical Characterization of SnO_2 and ITO Coatings

The optical absorption studies on ITO films were done using a Varian spectrophotometer (Model 17D). SnO_2 and ITO films were grown under identical growth conditions (CVD/CVD Spray) on quartz substrates. The quartz samples were located in the same zone as the aluminum samples which were used for corrosion testing. The absorption data results are shown in Figs. 10 and 11.

The bandgap of ITO (In/Sn ratio of 0.62) was found to be approximately 3.5 eV. In contrast, the SnO_2 film showed an energy gap of about 1.5 eV.

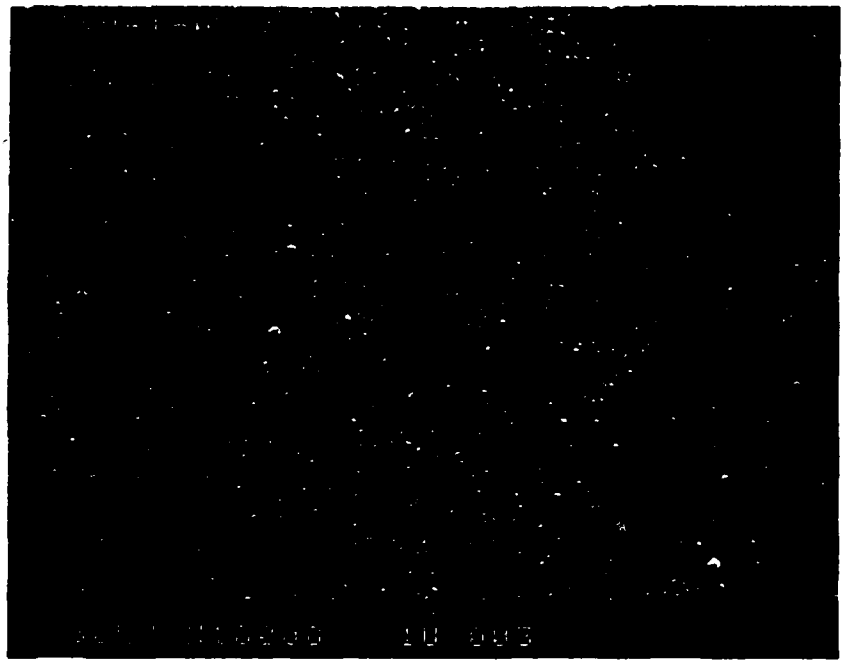

FIGURE 9a - SEM micrograph of CVD deposited ITO film

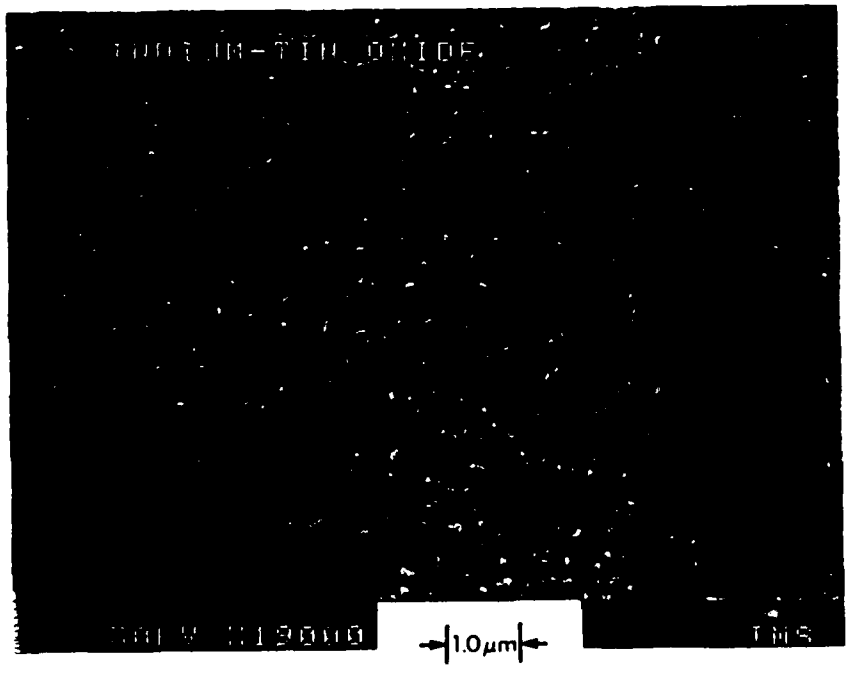

FIGURE 9b - SEM micrograph of spray CVD deposited ITO film

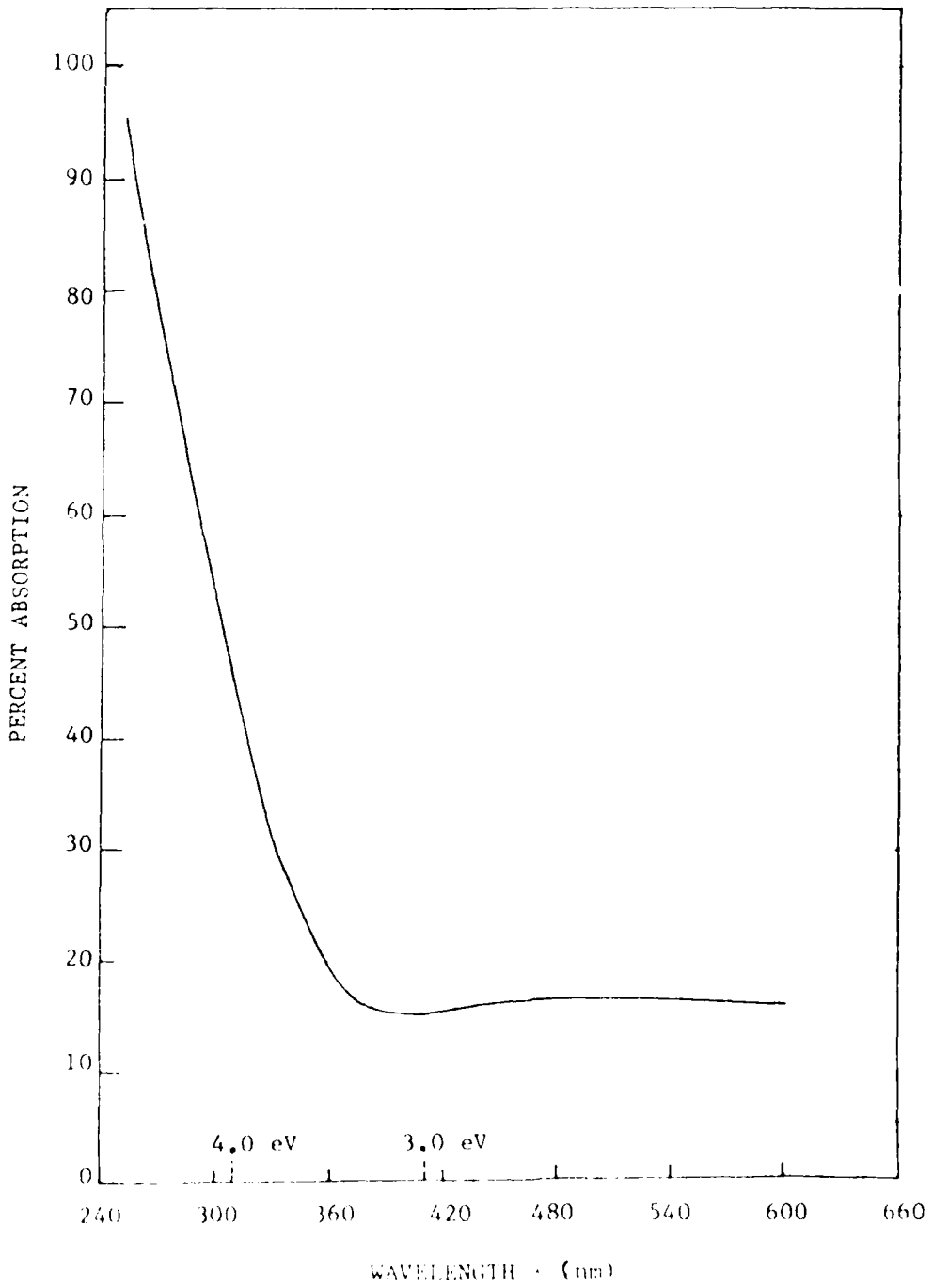

FIGURE 10 - The Absorption Edge of Indium Tin Oxide

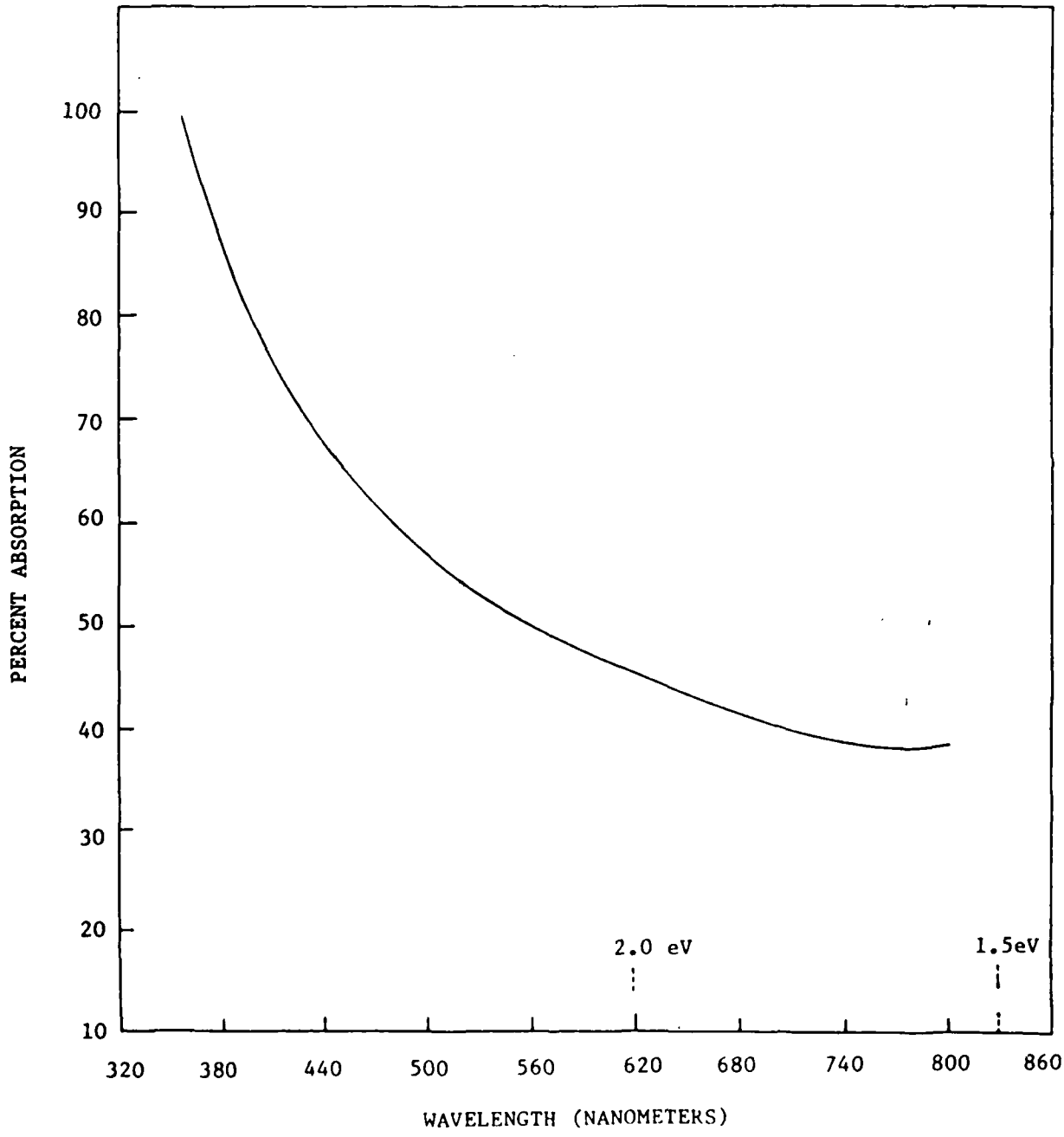

FIGURE 11 - The Absorption Edge of Tin Oxide

The optical data is a clear indication that the films are semiconducting. In addition, it shows that the energy bandgap is significantly larger in ITO.

IV.1.C Electronic Measurements

Resistivity Measurement

A four-point setup was used to determine the electrical resistivity of the ITO films. The tested ITO films included films grown in Si as well as quartz substrates. This technique does not work on ITO films grown on Al substrates as the aluminum, being a good conductor, interferes with the measurements. Table 3 lists the results of some resistivity measurements.

V-I Characteristics:

Direct evidence of the electronic barrier formation at Al/ITO interfaces was provided by analyzing voltage-current data of ITO/quartz samples.

Fig. 12 shows the arrangement used for voltage-current characteristics. ITO/quartz samples having Al and Ag deposited contacts were used. Here, the aluminum contact simulates the Al substrate (as in the Al/ITO samples used for corrosion testing) and Ag serves as the ohmic contact to the ITO film.

The V-I characteristics of two different (spray CVD) samples having In/Sn ratio of about 0.6 are shown in Figs. 13 and 14, respectively. Fig. 13 shows good rectifiction behavior ('REVERSE'), characteristic of a good electronic barrier. However, the 'FORWARD' characteristic seems to indicate series resistance (ohmic contact). Fig. 14 exhibits soft 'REVERSE' V-I characteristics, an indication of surface and/or defect states short-circuiting the barrier. The surface states provide an alternate path for current conduction, allowing part of the current to flow around the electronic barrier. Regardless, both samples verify the formation of the electronic barrier at Al/ITO interfaces. The absence of a barrier would result in a straight-line type of V-I plot under both forward and reverse biasing. Fig. 15 shows the V-I characteristics of an ITO/Si sample (prepared using the CVD technique) under dark and illuminated conditions. Computations based on dark voltage-current and photovoltaic measurements yielded an effective barrier height in the range of 0.15 - 0.4 eV.

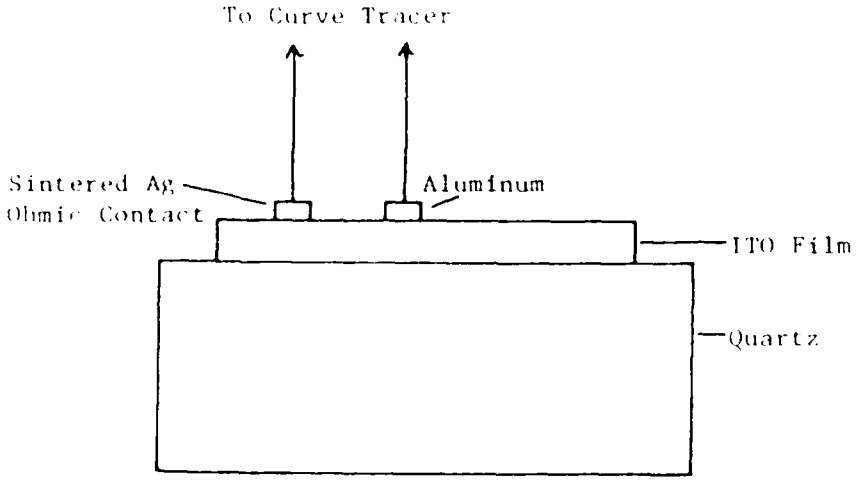

FIGURE 12 - V-I Characteristics Test Setup

TABLE 3 - Four-Point Probe Resistivity Measurements

Control Sample	Method of Deposition	ITO Conductivity Type	Resistivity Ω-cm	Growth Temp.°C
ITO/Si	Open Air Spray	n	3.7×10^{-3}	485
ITO/Si	Open Air Spray	p	5.9×10^{-3}	485
ITO/Si	Open Air Spray	n and p	8.5×10^{-3}	485
ITO/Si	CVD Spray	p	5.2×10^{-4}	460
ITO/Quartz	CVD Spray	n	3.6×10^{-4}	465
ITO/Quartz	Open Air Spray	n	5.9×10^{-3}	480

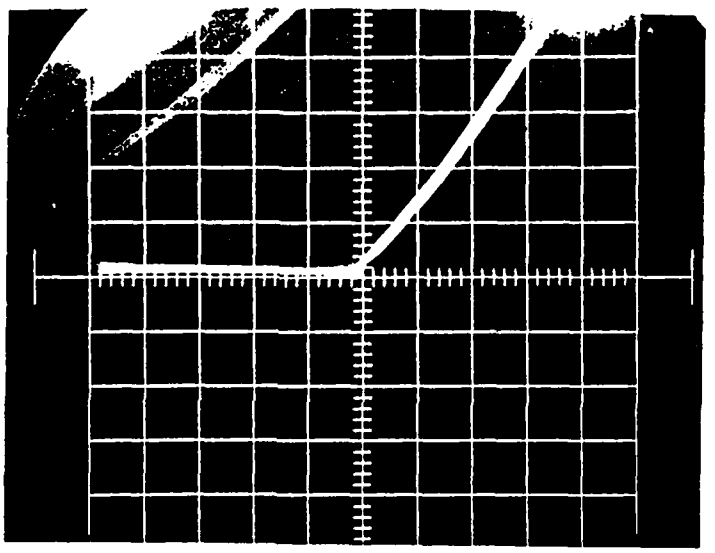

	FORWARD	REVERSE
CURRENT:	10 μA/DIV	10 μA/DIV
VOLTAGE:	0.5 V/DIV	0.5 V/DIV

Figure 13 -CURRENT-VOLTAGE CHARACTERISTIC OF AN Al-ITO/QUARTZ SAMPLE

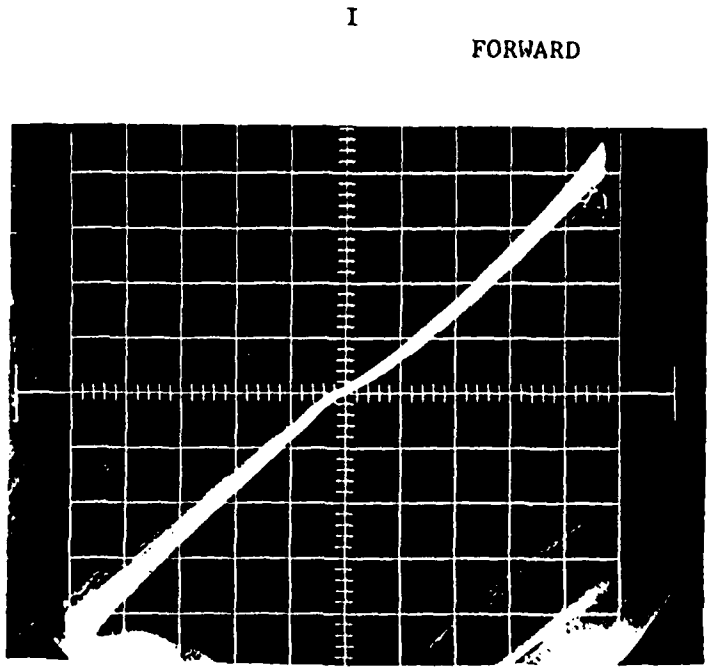

	FORWARD	REVERSE
CURRENT:	5 μA/DIV	5 μA/DIV
VOLTAGE:	0.5 V/DIV	0.5 V/DIV

Figure 14 -CURRENT-VOLTAGE CHARACTERISTIC OF AN Al-ITO/QUARTZ SAMPLE

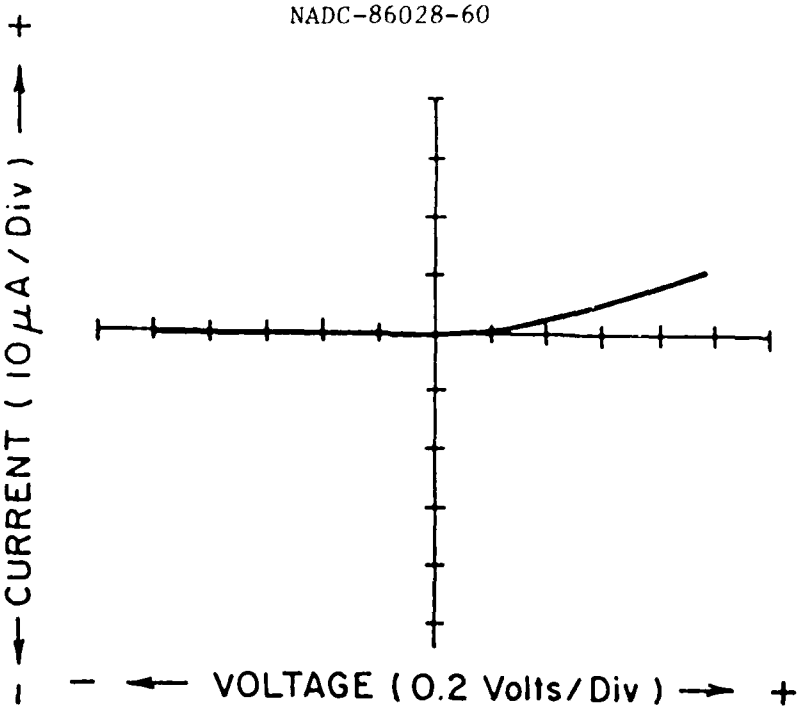

FIGURE 15a - Current-voltage characteristic of CVD Al-ITO sample (dark conditions)

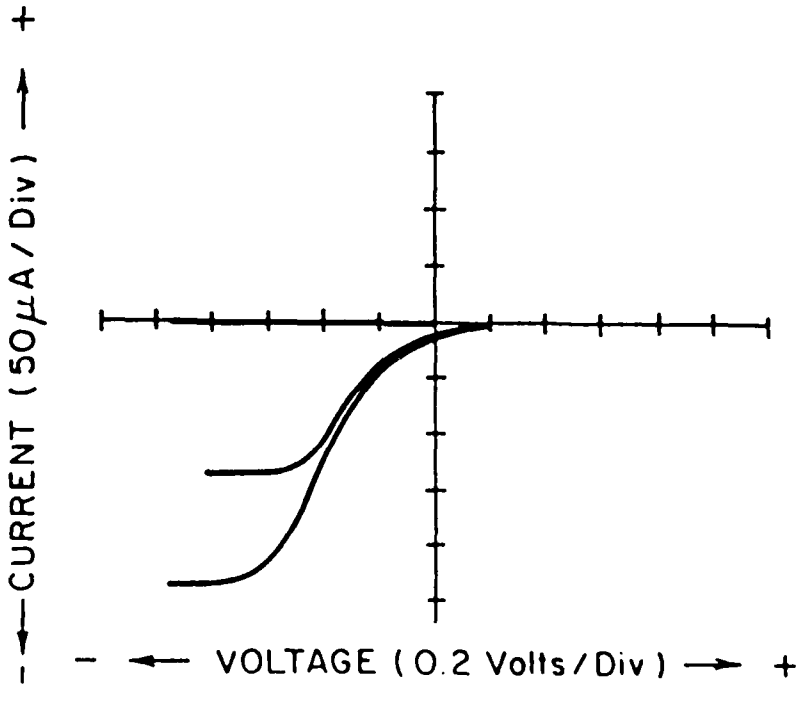

FIGURE 15b - Current-voltage characteristic of a CVD Al-ITO sample under illumination

IV. 2 Corrosion Testing

Fabricated structures were tested using weight-loss, and cathodic and anodic polarization techniques. A comparative study of various structures was conducted. The anodic polarization measurements were made at the NADC facilities using a potentiostatic setup. The details of this method are described elsewhere.[33] Table 4 summarizes some representative samples tested.

TABLE 4 - Anodic Polarization results (1% 2NaCl, 2pH)

Aluminum Type	Structure	Method of Growth	Resp Potential (-) Volt	Polarization results in Figure #
C.P.	Al-SiO_2-ITO	CVD Spray	0.980	16
C.P.	Al-SiO_2-ITO-Si_3N_4	Air Spray	0.845	16
C.P.	Al	Control Sample	0.72	16
H.P.	Al-Si_3N_4	Plasma	0.7	17
H.P.	Al-SiO_2-ITO	CVD Spray	0.66	17
H.P.	Al-SiO_2-ITO	Air Spray	0.707	17
Alloy	Al-SiO_2-ITO	CVD Spray	0.825	18
Alloy	Al-SiO_2-ITO	CVD Spray	0.9	18
C.P.	Al-SiO_2-ITO/TO-Si_3N_4	CVD Spray	0.833	19
C.P.	Al-SiO_2-ITO/TO-Si_3N_4	CVD Spray	0.965	20

C.P. = Commercial purity;

H.P. = High Purity;

Alloy = 7075-T6

Figs. 16-20 present polarization results on these samples. In all the voltage-current plots presented here, the point at the extreme left (intersecting the voltage axis) represents the rest potential. Fig. 21 shows polarization results of Al samples with low indium content ITO films. The role of the indium content will be discussed in the next section.

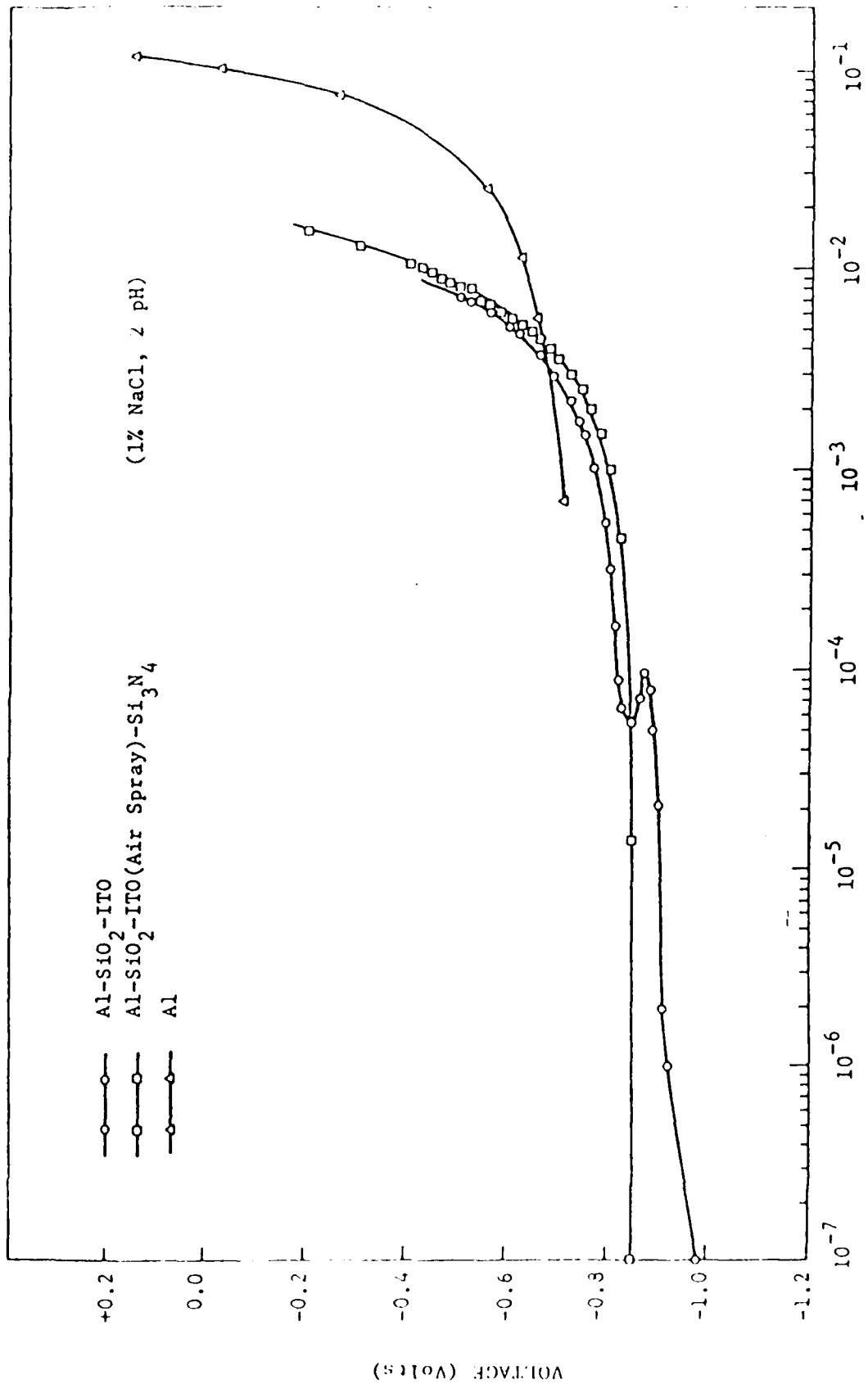

FIGURE 16 - Polarization characteristics of commercial purity aluminum substrates

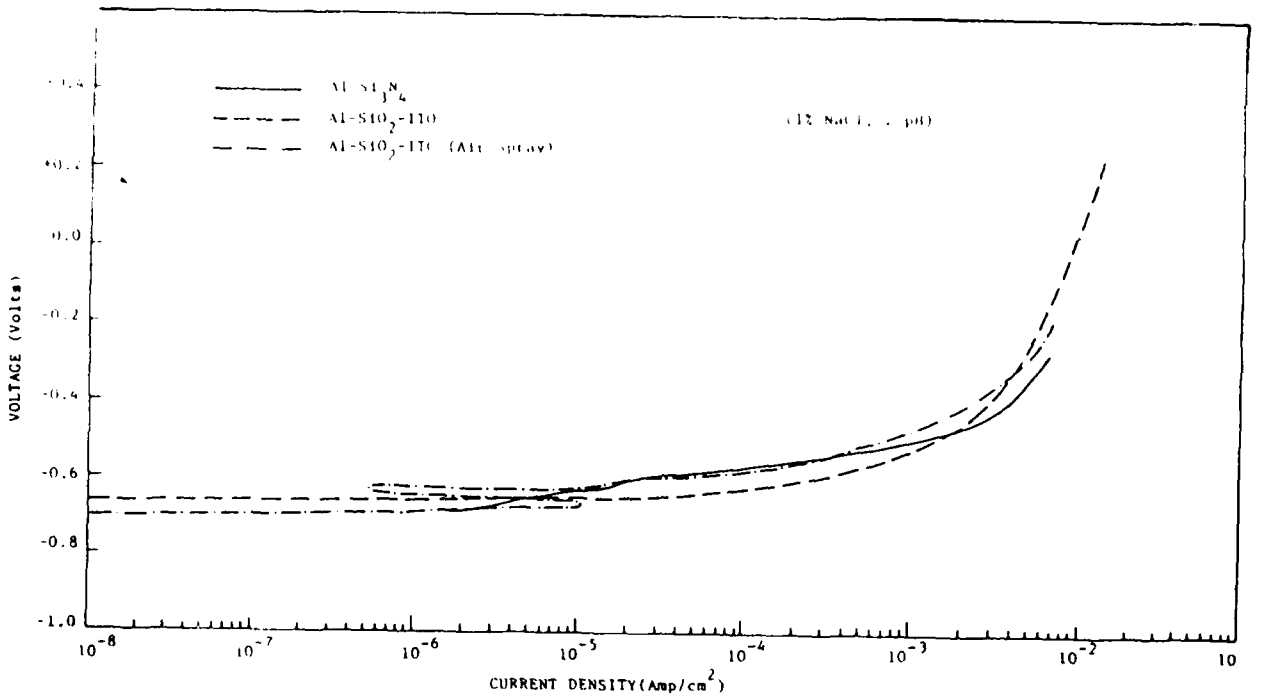

FIGURE 17 - Polarization characteristics of high purity aluminum substrates

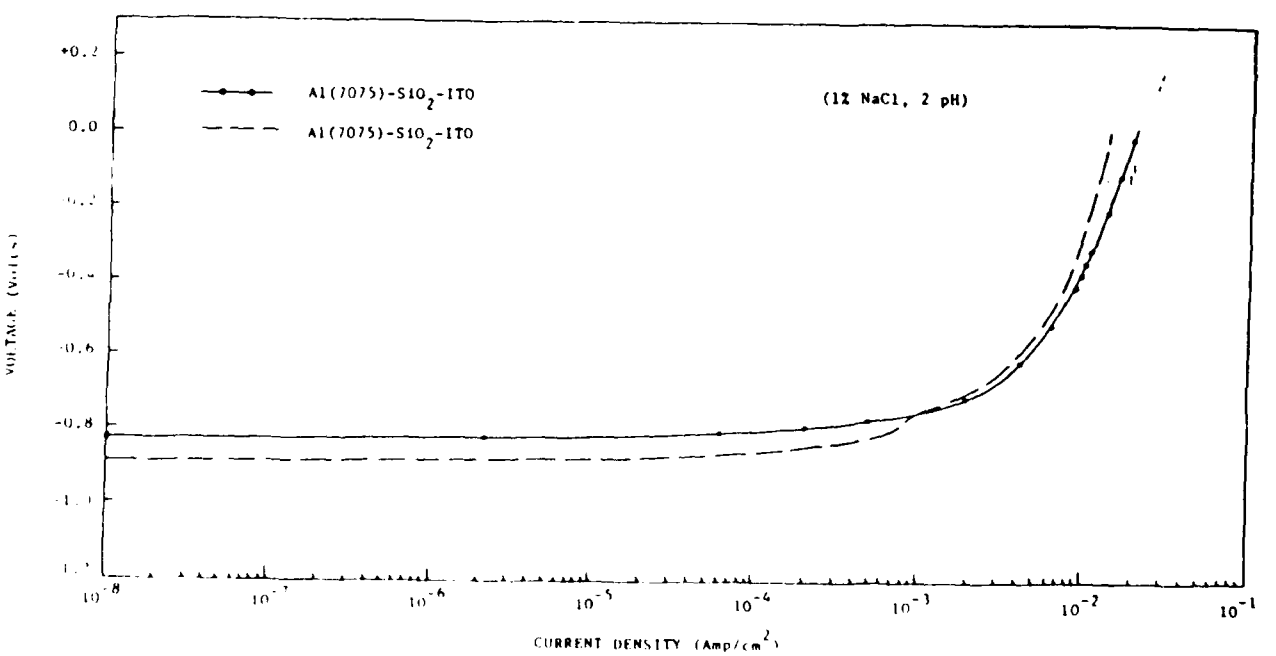

FIGURE 18 - Polarization characteristics of aluminum alloy (#7075-T6) substrates

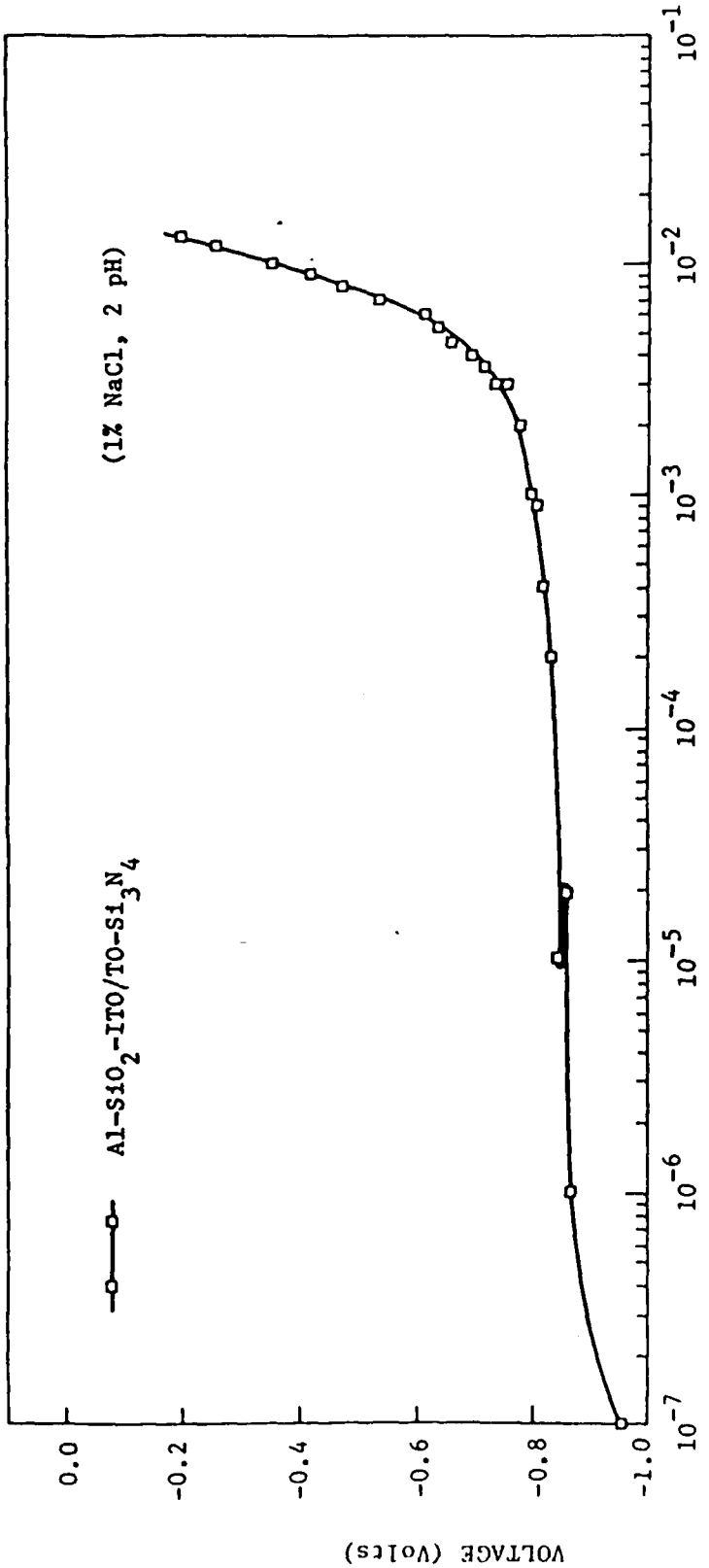

FIGURE 19 - Polarization Characteristic of a Commercial Purity Aluminum Substrate (With Composite ITO/TO Film)

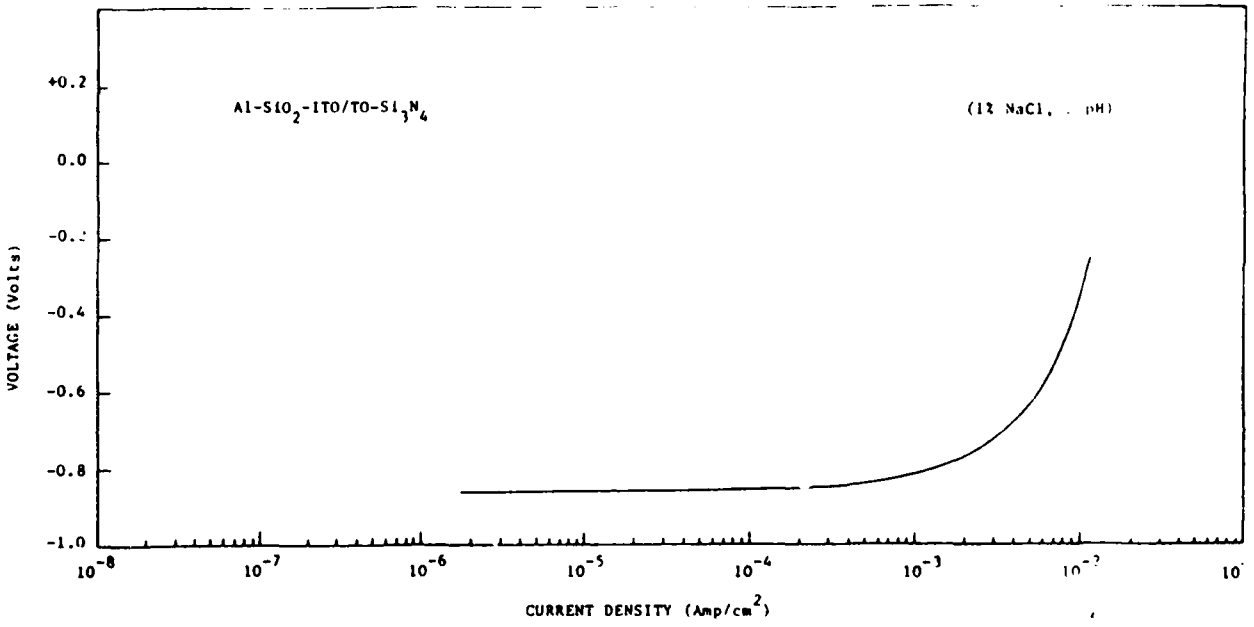

FIGURE 20 - Polarization characteristic of a scratched aluminum substrate (Commercial Purity)

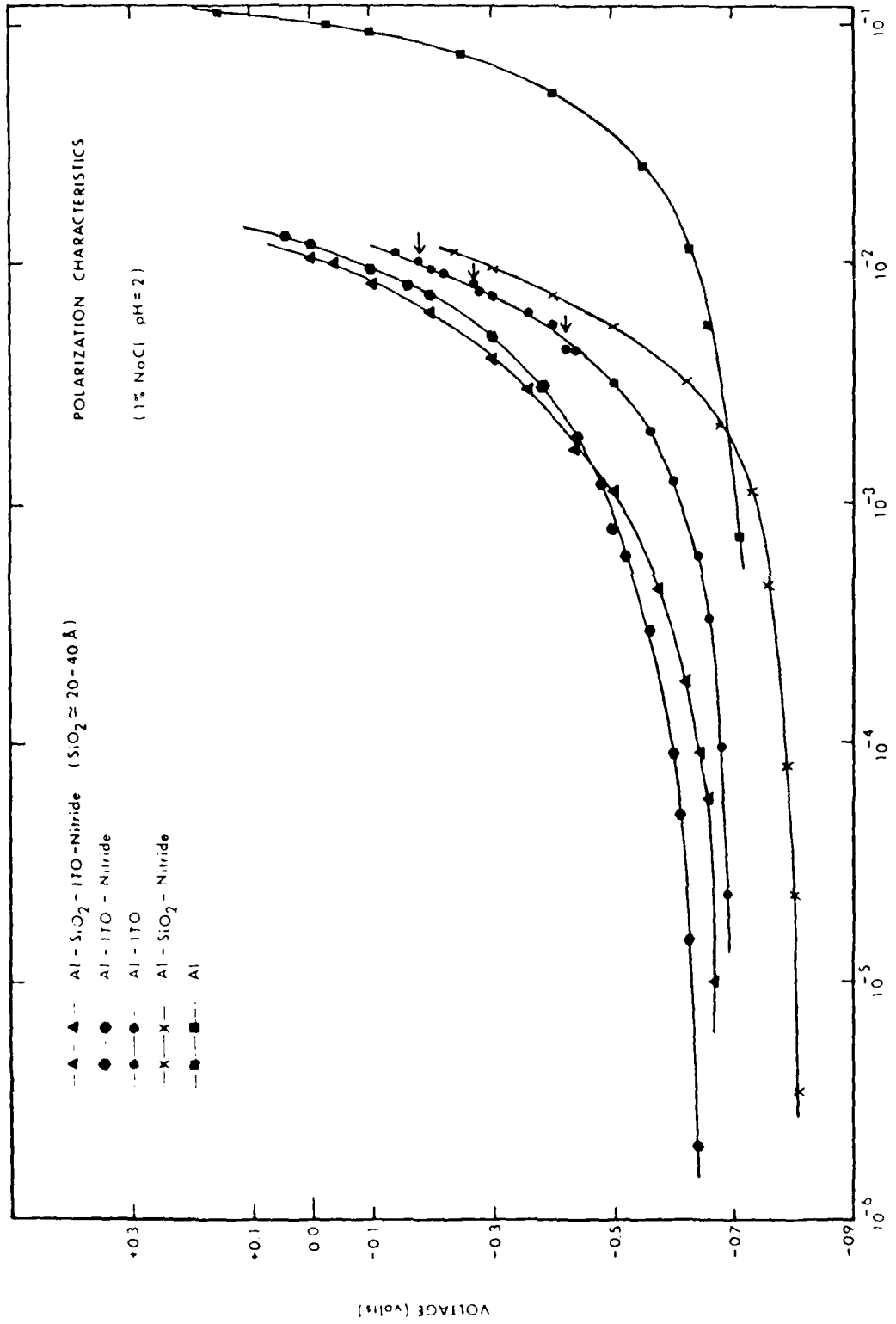

FIGURE 21 - Polarization characteristics of CVD deposited low indium content ITO samples

Weight-loss measurements were performed in our laboratory using 1-3% NaCl (with 2 pH) solutions. The weight loss measurements were conducted on Al-ITO samples coated with SiO_2 or Si_3N_4. The samples showed little or no weight loss. This data is shown in Table 5. High purity aluminum substrates were used for testing. The ITO films used in these samples were of low indium content. These films were grown in a CVD reactor.

TABLE 5.- Weight Loss Measurement on CVD Deposited Samples of Al in 3% NaCl Solution at pH 2

Sample #	Initial Wt gm	Wt after 70 Hrs. gm	Weight loss gm
Al-ITO-NITRIDE	2.08867	2.08863	0.00004
Al-ITO-SiO_2(THICK)	0.75436	0.75412	0.00024
Al	0.81532	0.81307	0.00225

[Surface area ≈ 5 cm^2]

The ITO films deposited by the spray deposition technique having higher indium content showed different weight loss results. Films deposited on quartz and mirror smooth silicon substrates showed negligible weight loss. For example, a typical Si sample (surface area ≈ 7.84 cm^2) coated with ITO having a total weight of 0.83714 gms showed no measurable weight-loss over a time period of 48 hours in a 1% NaCl solution (with pH=2). Similar results were found for ITO coated quartz samples. However, films deposited on commercial grade aluminum substrates exhibited hgiher weight losses. The rate of weight loss was small initially but accelerated with time.

V. DISCUSSION

This section interprets the results of the corrosion test data presented in the preceeding section. The anodic polarization data provides the most useful means of evaluating the protective nature of the ITO films. The significant increase in the magnitude of the rest potential in the presence of ITO semiconducting films is evident from Figs. 16-21. This increase, in conjuction with the electronic V-I characteristics, confirms the existence of the electronic barrier at the metal-semiconductor interfaces. Samples exhibiting higher magnitudes of rest potential also show reduced corrosion currents, particularly at lower voltages (i.e. within the range of 100 to 200 mV above the rest potential). Fig. 21 shows the importance of ITO as a protective coating in contrast to both SiO_2 and Si_3N_4 coatings. This figure compares unprotected Al, Al-passive films and Al-active barrier films. It should be mentioned that a relatively thick (0.7μm) plasma-deposited Si_3N_4 layer is not as protective as the much thinner (0.2μm) ITO layer. Additional comparisons of Al-Si_3N_4 films with Al-SiO_2-ITO and Al-SiO_2-ITO-Si_3N_4 films are given in Figs. 16 and 17. Another important feature evident from the comparative data is that the presence of a thin SiO_2 layer (50-100 Å) does indeed further increase the effective barrier height. This effect is evident in Figs. 16-21. The results also indicate that the SiO_2/ITO system is effective in protecting both aluminum (commercial and high purity Figs. 16, 17, 19-21) and aluminum alloy (Fig. 18) substrates.

A comparison of Fig. 21 with Figs. 16-20 illustrates the effect of indium content in the ITO films. The samples of Fig. 21 had lower indium-to-tin ratios (In/Sn ≈ 0.002) than thos of Figs. 16-21 (In/Sn ≈ 0.3-0.6). Clearly the polarization results of Figs. 16-20 show an increased magnitude in the rest potential and lower corrosion currents. This can be explained in terms of an increased electronic barrier at the Al-ITO interface with high In/Sn ratio films. It is well known that the electronic barrier at a metal-semiconductor interface increases with the energy gap of the semiconductor.[16] The ITO films containing more indium have been found to have an increased energy gap. This has been confirmed by the spectrophotometric measurements. The increased rest potential in the anodic polarization data has graphically demonstrated the importance of the semiconductor energy gap.

In addition to ITO coatings, composite coatings of ITO and tin oxide (TO) were also investigated. The motivation for this was twofold: (1) to increase the film thickness in order to minimize the occurrence of pinhole/micropores; and (2) to explore the possibility of a double active electronic barrier. The second barrier would exist at the ITO/TO heterointerface. Figs. 19 and 20 show these results. While these structures show promising results, further work is needed to characterize the properties of the second barrier.

The weight loss data for Al samples coated with ITO show different results for films deposited by CVD and spray deposition techniques. CVD deposited samples, having a low indium content, exhibit very low weight losses, as shown in Table 5. However, ITO films deposited by the injection spray technique show higher weight loss in spite of the higher active electronic barrier. This contradictory behaviour is attributed to the relatively poor surface qualities of the films grown by this method on Al substrates. Surface morphological analysis of weight-loss samples revealed that the weight loss was concentrated at selective sites. It is believed that these areas hosted large pinholes in the ITO films where selective undercutting occurred. Fig. 22 shows photographs of these area magnified by 420X. The substrates were commercial grade aluminum alloy (#7075-T6) with controlled ambient CVD spray deposited ITO films. The sequence of photographs dramatizes the growth of a pinhole due to undercutting at the pinhole site. It is further believed that the undercutting was reduced, if not eliminated, at small pinhole sites due to electric field fringing. Additional confirmation of this theory is provided by the weight loss results of Si-ITO and quartz-ITO samples. These results show that the spray deposited ITO films are indeed chemically impervious to the test environment.

We can further analyze the polarization data quantitatively. For instance, if we determine the change in current Δi for a small change in applied voltage $\Delta V = (V_{applied} - V_{Rest\ Potential})$, we can compare the effectiveness of the various coatings. If the change ΔV is less than 25 mV (i.e. $\frac{kT}{q}$; where k is the Boltzman Constant, q is the magnitude of electron charge, and T the temperature in Kelvin) we can obtain information on the intrinsic corrosion resistance of the film. Reference is made to Fontana and Greene[33] for additional details. Data extracted from the polarization measurements, particularly in the vincinity of rest potential (10 mV-20 mV), shows that the corrosion resistance was significantly greater than 10^8 ohms for the Al-SiO_2-ITO sample of Fig. 16 (the current change was less than 10 nA, and was not measured accurately on the setup used). In fact, it took a change of about

FIGURE 22 - Undercutting of ITO films at large pinhole sites

Pictures taken after exposure to 1% NaCl (2 pH) solution for following durations: a) 15 minutes, b) 45 minutes, c) 75 minutes, d) 105 minutes and e) 135 minutes. Magnification = 420X ; Scale : 1 cm = 24 μm

Figure 22a

Figure 22b

Figure 22c

Figure 22d

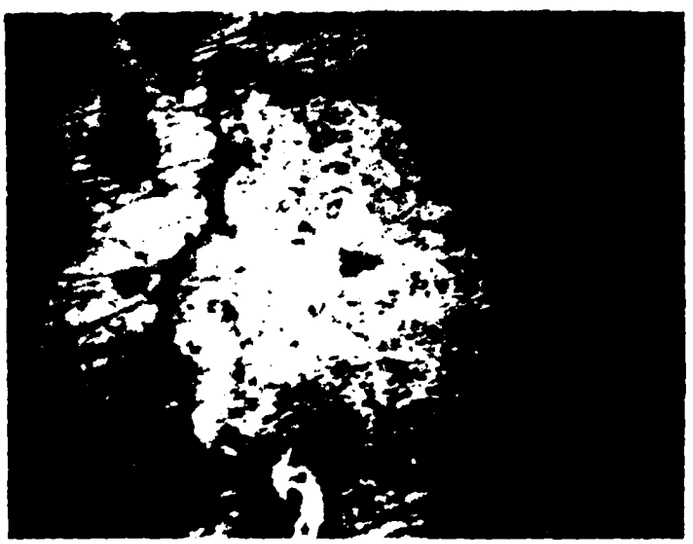

Figure 22e

0.1 volt to see a change of about 1 nA for this sample. Table 6 shows Δi versus ΔV for two samples having different compositions of ITO.

Table 6

Effect of Increased Indium Content in ITO

Sample	Growth Process	$\Delta V = \lvert V_A - V_{Rest} \rvert$ volts	Δi amps	In/Sn Ratio
Al-SiO_2-ITO	Spray Injection CVD ITO	0.06 0.10 0.20	1×10^{-6} 80×10^{-6} 0.78×10^{-3}	= 0.6
Al-SiO_2-ITO-Si_3N_4	CVD ITO	0.6 0.10 0.20	188×10^{-6} 430×10^{-6} 1.55×10^{-3}	0.002
Al-SiO_2-Si_3N_4	Plasma Deposited Nitride	0.06 0.10 0.20	385×10^{-6} 1185×10^{-6} 3.20×10^{-3}	

The change in current Δi for a given change in voltage ΔV has been found to be greater in the case of air-sprayed ITO in comparison to the CVD spray (see Fig. 16 and 17).

An important feature, observed in samples exhibiting incresed rest potential due to good ITO coatings, is the pheonmenon of currentlowering (passivation) in spite of an increase in the applied voltage. This is observed in Fig. 16 (Al-SiO_2-ITO sample), Fig. 17 (Al-SiO_2-ITO) and Fig. 19 (Al-SiO_2-ITO/TO/Si_3N_4 sample).

VI. CONCLUSIONS

The use of an active electronic barrier in corrosion prevention is a novel concept[17], and the validity of this approach has been demonstrated using Al-ITO and Al-SiO_2-ITO samples. The protective nature of the active electronic barrier in Al-SiO_2-ITO films is clearly evident when the polarization

results of these samples are compared with Al-Si_3N_4 (plasma-deposited) passive structures. The ITO coated samples with a film thickness of only 0.2 microns yielded lower currents than the Si_3N_4 coated (0.75 microns) samples. Weight-loss measurements further verify the concept of an active electronic barrier for use in corrosion prevention.

ITO films containing more indium have been found to have an increased electronic barrier at the Al/ITO interface. This has been shown in both the voltage-current characteristics and the anodic polarization data. The increased rest potential in the anodic polarization data has confirmed the increased active barrier with In rich films. The increase in the indium content has clearly shown a corresponding increase in the energy gap of the ITO films. This has been confirmed by spectrophotometeric measurements.

A commercially viable processing system has been simulated by the deposition of ITO films using an injection spray technique. This has been done in a controlled ambient as well as in air. Results of the controlled ambient system have been better than the air spray system, and quite comparable to the chemical vapor deposition technique developed earlier in our laboratory. However, further process optimization is required to obtain high quality ITO films with a minimum number of pinholes.

The concept of active electronic barriers could also be applied to other semiconductor coatings on metals such as silicides, doped polyacetylene, pthalocyanine, chlorophyll, porphyrins, etc.

VII. FUTURE WORK

A. Controlled Doping of ITO

High quality films of ITO and SnO_2 have been grown in both n and p-type dopings. However, the control over the amount of doping, necessary to obtain high resistivity films of n and p-type, has been poor. Current films of each type exhibit low resistivities (10^{-2} to 10^{-3} Ω .cm). These low resistivity films do form an effective electronic barrier at the aluminum surface, however, the corrosion protection can be further enhanced by increasing the film resistivity.

In addition, the controlled doping will allow for the optimization of the active electronic barrier.

B. Growth of Thicker Homogeneous Films

The growth of thicker ITO films (> 1.0μm) is necessary to minimize the occurrence of microscopic pinholes. Extremely uniform films of ITO Have been grown on Si wafers using the CVD spray deposition system. However, ITO films grown on aluminum substrates have been of lower quality. It is suspected that it is due to rapid cooling of the aluminum surface during the spray deposition. Additional work is needed in the reactor design to improve film quality and homogeneity.

C. Current Transport Modeling

A theoretical model of the current transport in Al-SiO_2-ITO structures is needed to characerize the effective height of the barrier formed at the interface.

A relationship to predict effective barrier height in terms of the ITO energy gap E_g and the location of defect trap levels is needed. This model will be general enough to be of use for other systems such as Al-polyacetylene, Al-phthalocyanine, etc. The model would also be used to obtain relationships for the corrosion current. In addition, the nature of the ITO-electrolyte interface (as in polarization testing) must be studied. This information would be useful in understanding the effects of the ITO-ambient interface.

D. Investigation of Multiple ITO/TO Coatings

Preliminary investigation suggests that the semiconductor heterointerface formed between ITO and SnO_2 layers results in a second active electronic barrier which enhances the corrosion resistance. Further work is needed to characterize this phenomena.

A C K N O W L E D G E M E N T S

The author wishes to acknowledge J. J. Rosato and K. S. Kalonia for their assistance during the course of this study. Thanks are due to Dr. V. S. Agarwala for helpful discussions and avowed interest in the project. He is grateful to J. G. Bouchard(Sprague Electric Company, Worcester, MA) for the deposition of nitride films.

REFERENCES

1. J.C. Scully, The fundamentals of corrosion, Pergamon, New York (1975).

2. A. Bianconi, "Study of the initial oxidation of single crystal aluminum by inter-atomic Auger Yield Spectroscope," Solid State Comm., 24, 539 (1977).

3. H.L. Yu, M.C. Munoz, and F. Soria, On the initial stages of oxidation of A1 (111) by LEED analysis, Surface Science, 94, L184 (1980).

4. B.W. Bullett, The bonding of oxygen to A1 (111), Surface Science, 93, 213-222 (1980).

5. J.A. Appelbaum, Electronic structure of solid surfaces, Chapter 2, in Surface physics of materials, Vol. 1, Ed. J. M. Blakely, Academic Press, N.Y. (1975).

6. M. C. Munoz, V. Martinez, J. A. Tagle, and L. D. Sacedon, Observation of Surface Stastes in the Auger spectra of Clean and oxygen chemisorbed Si(111) 7x7, Phys. Rev. Lett. 44, 814.

7. S. Roy Morrison, The chemical physics of surfaces, Plenum Press, New York, 1977; also in Surface Physics of Phosphors and semiconductors (chapter 4), Eds. C.G. Scott and C.E. Reed, Academic Press, New York (1975).

8. J.R. Schreiffer and P. Soven, Phys. Today, 28, 24 (1975).

9. N.D. Tomashov, Theory of corrosion and protection of metals, MacMillan, New York (1966).

10. K. Barton, Protectrion against atmospheric corrosion: Theoreis and Methods, Wiley Interscience, New York (1976).

11. V.E. Carter, Metallic coatings for corrosion control, Newnes-Butterworths, Boston (1977).

12. C. Wagner, The formation of thin oxide films on metals, Corrosion Science 13, 23-52 (1973).

13. K. Schneider, R. Bauer, and H.W. Grunling, "Corrosion and Failure mechanisms of coatings for gas turbine applications", Thin Solid Films, 54, 359-367 (1978).

14. A.T. Fromhold, Theory of Metal Oxidation, Vol. 1 - Fundamentals. In Series on Defects in crystalline solids, Vol. 9, North-Holland (1976).

15. A.T. Fromhold, Theory of metal oxidation, Vol. 2 - Space charge, in Series on Defects in solids, Volume 12, North-Holland (1980).

16. S.M. Sze, Physics of semiconductor devices, second edition, John Wiley, New York (1981).

17. F.C. Jain, Semiconductor/Insulator Films in Corrosion Prevention, Private Communication to U.S. Naval Air Development Center, September (1980).

18. A.G. Milnes and D.L. Feucht, Heterojunctions and Metal-Semiconductor junctions, Academic Press, N.Y. (1972).

19. R.S. Muller and T.I. Kamins, Device electronics for integrated circuits, Wiley, N.Y. (1977).

20. J.M. Andrews and J.C. Phillips, Chemical bonding and structure of metal-semiconductor interfaces, Phys. Rev. Lett. 35, 56 (1975).

21. L.J. Brillson, Chemically induced charge redistribution at A1-GaAs interfaces, Phys. Rev. Lett. 42, 397 (1979).

22. G. Ottaviani, K.N. Tu and J.W. Mayer, Interfacial reaction and Schottky barrier in metal-silicon system, Phys. Rev. Lett. 44, 284 (1980). (Reference is made of the Proceedings of Conference on Physics and Chemistry of Semiconductor Interfaces (PCSI), 1983, 1984).

23. A. Goetzberger, E. Kalusmann, and M.J. Schulz, Interface states on semiconductor/insulator surfaces, CRC Critical Rev. in Solid State Sciences, 6, 1-45 (January 1976).

24. E.H. Nicollian, B. Schwartz, D.J. Coleman, Jr., R.M. Ryder, and J.R. Brews, Influence of thin oxide layer between metal and semi-conductor on Schottky diode behavior, J. Vac. Sci. Technol., 13, 1047.

25. F.C. Jain and J.W. Marciniec, A single-heterostructure MOS injection laser, IEEE J. Quantum Electronics, QE-14, 398 (1978).

26. F.C. Jain and C.S. Nichols, Electronic transport and emission of light in Au-SiO_2-GaAsP interfaces. Bull. Am. Phys. Co. 25, 586 (1979).

27. J.P. Dodelet, Characteristics and behavior of electrodeposited surfactant phthalocyanine photovoltaic cells, J. Appl. Phys. 53, 4270-4277, June 1982.

28. N. Koshida and Y. Wachi, Application of ionimplanation for doping of polyacetylene films, Appl. Phys. Lett. 45, 436-437, August 1984.

29. M. Froment, Passivity of Metals and semiconductors, Elsevier (1983). (Proceedings of the Fifth Internation Symposium on Passivity, Bombanness France, May 30-June 3, 1983).

30. F.C. Jain, Technical Report to NADC entitled "Formation of Electronic Barrier at A1-semiconductor Interfaces: A New Approach to Corrosion Prevention" (contract #N62269/83-66-32008) August 1985.

31. S. Ashok, P. Sharma, and S. Ponash, Spray-deposited ITO-Si SIS heterojunction solar cells, IEEE Transd. Electron Dev. ED-27, 725 (April 1980).

32. E.L. Jordan, A diffusion mask of SiO_2, J. Electrochem, Soc. 108, 478 (1961).

33. M.G. Fontana and N.D. Greene, Corrosion Engineering, McGraw-Hill, New York (1978).

DISTRIBUTION LIST (continued)

	No. of Copies
Dr. C. McMahon, LRSM University of Pennsylvania Philadelphia, PA 19104	1
Defense Technical Information Center Attn: DTIC-DDA-1 Cameron Station, Bldg. 5 Alexandria, VA 22314	12
NAVAIRDEVCEN (3 for Library - 8131) (50 for U.S. Agarwala - 6062)	53

DISTRIBUTION LIST (continued)

	No. of Copies
Naval Underwater Systems Center (Code 4493) New London, CT 06320 (Dr. R. G. Kasper)	1
AFOSR, Bolling AFB Washington, DC 20332 (Dr. A. Rosenstein)	1
Wright-Patterson AFB WPAFB (AFWAL/MLSA) OH 45433 (Mr. B. Cohen)	1
Air Force Logistics Center (MMEMC) Warner-Robbins AFB Warner, GA 31098 (Mr. W. Thompson)	1
Army Research Office P.O. Box 12211 Research Triangle Park; NC 27709 (Dr. R. Reeber)	1
U.S. Army Materials and Mechanics Research Center, (DRXMR-EM), Watertown, MA 02172 (Dr. M. Levy)	1
U.S. Army Armament R&D Command (DRDAR-SCM) Bldg. 355, Dover, NJ 07801	1
U.S. Army Mobility Equipment R&D Command (DRDME-VC) Fort Belvoir, VA 22060 (Mr. D. A. Emeric)	1
National Bureau of Standards Washington, DC 20234	1
Dr. H. Leidheiser, Jr. Center for Coatings and Surface Research Lehigh University Bethlehem, PA 18015	1
Dr. M. Kendig Rockwell International Science Center 1049 Camino Dos Rios, P.O. Box 1085 Thousand Oaks, CA 91360	1

DISTRIBUTION LIST (continued)

	No. of Copies
Commander Naval Air Force U.S. Atlantic Fleet Attn: Code 5281 Norfolk, VA 23511	1
Commander Naval Air Force U.S. Pacific Fleet Attn: Code 7412 San Diego, CA 92135	1
Naval Sea Systems Command Washington, DC 20362	1
Chief of Naval Material Navy Department Washington, DC 20350	1
Office of Naval Research 800 N. Quincy St. Arlington, VA 22217 (Dr. A. J. Sedriks)	1
Office of Naval Technology NAVMAT-0725 800 N. Quincy St. Arlington, VA 22217 (Mr. J. J. Kelly)	1
Naval Research Laboratory 4555 Overlook Ave. Washington, DC 20375 (Mr. J. Good)	1
David Taylor Ship Research Development Center Code (281) Annapolis, MD 21402 (Mr. A.G.S. Morton, Mr. G. Wacker)	2
Naval Surface Weapons Center (Code R-30) White Oak Silver Spring, MD 20910	1
Naval Air Propulsion Center (Code PE-72) Trenton, NJ 08628 (Mr. A. J. Dorazio)	1

DISTRIBUTION LIST
REPORT NO. NADC-86028-60

	No. of Copies
Naval Air Systems Command (2 for AIR-7226) (1 for AIR-31A) (2 for AIR-5304) (1 for AIR-5142) (1 for AIR-03D)	6
Commanding Officer Naval Air Rework Facility Attn: Code (340) Naval Air Station Alameda, CA 94501	1
Commanding Officer Naval Air Rework Facility Attn: Code (340) Naval Air Station Jacksonville, FL 32212	1
Commanding Officer Naval Air Rework Facility Attn: Code (340) Naval Air Station Norfolk, VA 23511	1
Commanding Officer Naval Air Rework Facility Attn: Code (340) Naval Air Station North Island San Diego, CA 92135	1
Commanding Officer Naval Air Rework Facility Attn: Code (340) Naval Air Station Pensacola, FL 32508	1
Commanding Officer Naval Air Rework Facility Attn: Code (340) Marine Corp. Air Station Cherry Point, NC 28533	1

END

DTIC

7-86